NPS-PH-01-001

NAVAL POSTGRADUATE SCHOOL
Monterey, California

Free Electron Laser
Material Damage Studies

By

R. D. McGinnis, R. W. Thomson, L. R. Short, P. A. Herbert,
D. Lampiris, A. Christodoulou, W. B. Colson
Naval Postgraduate School

and

M.D. Shinn, G. Neil, S. Benson,
J. Gubeli, R. Evans, K. Jordan
Thomas Jefferson National Accelerator Facility

November 2000

Approved for public release; distribution is unlimited.

Prepared for: Naval Postgraduate School
Monterey, CA 93943-5000

20001222 097

DTIC QUALITY INSPECTED 4

Naval Postgraduate School

Monterey, California 93943-5000

RADM David R. Ellison, USN
Superintendent

Richard Elster
Provost

This report was prepared for Naval Postgraduate School.

Prepared by: Roger D. McGinnis

Roger D. McGinnis
Commander USN

Prepared by: W. B. Colson

William B. Colson
Distinguished Professor of Physics

Reviewed by: William B. Maier II

William Maier, Chairman
Department of Physics

Released by: for Distinguished Professor David W. Netzer
Associate Provost and Dean of Research

REPORT DOCUMENTATION PAGE

Form Approved
OMB No. 0704-0188

Public reporting burden for this collection of information is estimated to average 1 hour per response, including the time for reviewing instruction, searching existing data sources, gathering and maintaining the data needed, and completing and reviewing the collection of information. Send comments regarding this burden estimate or any other aspect of this collection of information, including suggestions for reducing this burden, to Washington headquarters Services, Directorate for Information Operations and Reports, 1215 Jefferson Davis Highway, Suite 1204, Arlington, VA 22202-4302, and to the Office of Management and Budget, Paperwork Reduction Project (0704-0188) Washington DC 20503.

1. AGENCY USE ONLY *(Leave blank)*	2. REPORT DATE November 2000	3. REPORT TYPE AND DATES COVERED Technical Report

4. TITLE AND SUBTITLE
Free Electron Laser Material Damage Studies

5. FUNDING NUMBERS

6. AUTHOR(S)
McGinnis, R.D., Thomson, R.W., Short, L.R., Herbert, P.A., Lampiris, D., Christodoulou, A., Colson, W.B., M.D. Shinn, G. Neil, S. Benson, J. Gubeli, R. Evans, K. Jordan

7. PERFORMING ORGANIZATION NAME(S) AND ADDRESS(ES)
Naval Postgraduate School
Monterey, CA 93943-5000

8. PERFORMING ORGANIZATION REPORT NUMBER
NPS-PH-01-001

9. SPONSORING / MONITORING AGENCY NAME(S) AND ADDRESS(ES)

10. SPONSORING / MONITORING AGENCY REPORT NUMBER

11. SUPPLEMENTARY NOTES
The views expressed in this thesis are those of the authors and do not reflect the official policy or position of the Department of Defense or the U.S. Government.

12a. DISTRIBUTION / AVAILABILITY STATEMENT
Approved for public release; distribution unlimited.

12b. DISTRIBUTION CODE

13. ABSTRACT

Today's surface ships are faced with an increased vulnerability to anti-ship cruise missiles, due to a change from operating in open oceans to primarily operating in the world's littorals. One possible solution to counter this threat is the use of a high-energy laser to destroy the missiles in flight. The Free Electron Laser is possibly the best choice of lasers for a marine environment since its wavelength can be changed over a wide range allowing the operator to choose the best wavelength to transmit through the atmosphere. Material damage studies on various anti-ship cruise missile materials were carried out at Thomas Jefferson National Accelerator Facility (TJNAF) in Newport News, Virginia. Experimental procedures presented in this report allow a scaled down laser of a few hundred to a few thousand watts to evaluate the damage from a weapon size laser of the megawatt class. The FEL beam bombards the target with a steady stream of picosecond length pulses at rates of 18MHz or greater. No other experiments have previously been done to explore the effects of the FEL pulse on materials. This report contains the work of several theses conducted at the Naval Postgraduate School over the past two years, and has been a productive cooperation among NPS, TJNAF, NRL, and NSWD at Port Hueneme, to the benefit of the Department of Defense.

14. SUBJECT TERMS
Free Electron Laser, Laser Damage, Anti-Ship Cruise Missiles

15. NUMBER OF PAGES
110

16. PRICE CODE

17. SECURITY CLASSIFICATION OF REPORT	18. SECURITY CLASSIFICATION OF THIS PAGE	19. SECURITY CLASSIFI- CATION OF ABSTRACT	20. LIMITATION OF ABSTRACT
Unclassified	Unclassified	Unclassified	UL

NSN 7540-01-280-5500

Standard Form 298 (Rev. 2-89)
Prescribed by ANSI Std. 239-18

EXECUTIVE SUMMARY

This report is a consolidation of results from material damage studies reported in six theses conducted by students at the Naval Postgraduate School [Refs: 1 through 6]. The experiments were carried out between March 1999 and March 2000, at the Department of Energy's Thomas Jefferson National Accelerator Facility (TJNAF) in Newport News, Virginia. TJNAF has developed a 1.7 kW Free Electron Laser (FEL), with plans to increase the power to tens of kilowatts in the near term, and hundreds to thousands of kilowatts in the far term.

The primary purpose of these studies was to investigate the material damage effects caused by a Free Electron Laser (FEL). The materials used in the experiments included aluminum, as well as five different types of materials used in missile radomes.

One aspect to be explored was the potential effect on various materials resulting from the very short radiation pulses and high pulse repetition rate of the TJNAF FEL. Previous studies have shown that for high energy short pulses, additional damage (beyond the thermal damage) can result if the fluence per pulse is high enough.

Scaling laws for the lasers effect on the various missile radome materials was sought in order to allow the results from small scale experiments to be extrapolated to full size material damage results.

The studies indicate that consistent damage predictions can be made for low power lasers on small scale targets, provided the laser spot size is larger than the thermal diffusion length. The thermal diffusion length is a parameter of the material being irradiated, and indicates just how fast heat conducts away from the irradiated spot into the surrounding material. If the heat conduction is fast, the thermal diffusion length is large, and the laser spot size must be large enough to raise the material to the melting temperature before the heat diffuses away. The thermal diffusion requirement is necessary to ensure that small scale results mimic real world results where the laser spots would far greater than almost any materials thermal diffusion length.

The experiments included airflow across the targets to simulate the effect of airflow across the missile nose cone. The studies seem to indicate that the airflow does two things. First, it helps to remove smoke, debris, and sometimes melted material from the area of the laser spot. However, it can also cool the spot, resulting in a longer burn through time for some of the materials tested.

Another important result obtained in these experiments concerns the change in thermal diffusion length that can accompany a change in state of the material. One of the materials had a small thermal diffusion length in its original solid state, but once it melted, the thermal diffusion length appeared to grow dramatically. The heat

was carried away before it could further damage the target. This result indicates how important it is for the energy to be delivered to the target on a large enough spot size and at a high enough intensity to avoid thermal diffusion.

A third observation was with the higher fluence short pulses generated by the lower pulse repetition rate experiments. These higher fluence pulses may have enough energy to cause immediate vaporization (ablation) of the material being irradiated. When this happens the material is immediately removed and thermal diffusion cannot take place leading to a faster burn through rate. However, the pulses used in these experiments were very close to the ablation threshold, so that the benefits of the higher fluence short pulses was marginal.

Finally, the experiments validated estimates for predicting the amount of energy needed to destroy a target. These predictions do not include thermal diffusion, and proved to be more accurate at higher intensity levels where thermal diffusion is not as important.

TABLE OF CONTENTS

I. INTRODUCTION 1

A. LASER WEAPONS 1

II. LASER MATTER INTERACTION THEORY AND PREDICTIONS 3

A. REQUIRED POWER TO DESTROY TARGET 4

B. SCALING LAWS AND MINIMAL SPOT SIZE 8

C. PULSE TRAIN 9

D. ULTRA-SHORT PULSES 11

III. TJNAF FACILITY 15

A. TJNAF FEL 15

B. USER LAB 17

IV. MATERIALS 21

A. MATERIALS USED IN EXPERIMENTS 21

B. THERMAL DIFFUSION CALCULATIONS 22

V. MATERIAL DAMAGE EXPERIMENTS 24

A. EXPERIMENTAL PROCEDURES 24

1. March 1999 ..... *24*

2. August 1999 ..... *26*

3. March 2000 ..... *27*

B. EXPERIMENTAL RESULTS 29

1. Phenolic Resin *29*

2. Pyroceram *37*

3. Slip-Cast Fused Silica *41*

4. Polyimide Fiberglass *62*

5. F2 Epoxy *76*

VI. CONCLUSIONS **89**

A. SCALING 89

B. FEL PULSE FORMAT 90

C. FUTURE EXPERIMENTS 91

VII. REFERENCES **93**

VIII. INITIAL DISTRIBUTION **95**

LIST OF FIGURES

FIGURE 1. FEL PULSE FORMAT. 10

FIGURE 2. CURRENT FEL CONFIGURATION. 16

FIGURE 3. UPGRADED FEL CONFIGURATION. 16

FIGURE 4. OPTICAL BENCH. 18

FIGURE 5. FRONT VIEW OF OPTICAL BENCH. 19

FIGURE 6. REAR VIEW OF OPTICAL BENCH. 19

FIGURE 7. IRRADIANCE VS. DISTANCE FROM FOCAL POINT. 25

FIGURE 8. PHENOLIC RESIN SAMPLE 1. 30

FIGURE 9. PHENOLIC RESIN SAMPLE 1, RUN 2. 32

FIGURE 10. PHENOLIC RESIN SAMPLE 2. 33

FIGURE 11. PHENOLIC RESIN SAMPLE 2, RUN 3. 35

FIGURE 12. PHENOLIC RESIN SAMPLE 2, RUN 6. 36

FIGURE 13. PYROCERAM SAMPLE 1 38

FIGURE 14. PYROCERAM SAMPLE 2 39

FIGURE 15. SLIP-CAST FUSED SILICA SAMPLE. 41

FIGURE 16. EXPOSURE TIME VS. PENETRATION DEPTH RATE FOR FUSED SILICA. 43

FIGURE 17. CLOSE-UP OF DAMAGE TO SLIP-CAST FUSED SILICA RUN 2. 44

FIGURE 18. SKETCH OF BEAM FOCUSING EFFECT. 45

FIGURE 19. SEM PHOTOGRAPH OF DAMAGE TO FUSED SILICA RUN 7. 46

FIGURE 20. SLIP-CAST FUSED SILICA SAMPLE 1. 50

FIGURE 21. CLOSE-UP DAMAGE TO SLIP-CAST FUSED SILICA RUN 2. 51

FIGURE 22. SLIP-CAST FUSED SILICA SAMPLE 2. 52

FIGURE 23. EXPOSURE TIME VS. PENETRATION RATE FOR FUSED SILICA MARCH 1999. 54

FIGURE 24. SLIP-CAST FUSED SILICA SAMPLE 3. 56

FIGURE 25. CLOSE-UP OF DAMAGE OF SLIP CAST FUSED SILICA RUN 1. 61

FIGURE 26. CLOSE-UP OF DAMAGE OF SLIP-CAST FUSED SILICA RUN 2. 61

FIGURE 27. BACK VIEW OF DAMAGE TO SLIP CAST FUSED SILICA RUNS 1 AND 2. 62

FIGURE 28. POLYIMIDE FIBERGLASS. 62

FIGURE 29. CLOSE-UP OF DAMAGE TO POLYIMIDE FIBERGLASS RUN 1. 64

FIGURE 30. CLOSE-UP OF DAMAGE TO POLYIMIDE FIBERGLASS RUN 2. 64

FIGURE 31. CLOSE-UP OF DAMAGE TO POLYIMIDE FIBERGLASS RUN 3. 65

FIGURE 32. POLYIMIDE FIBERGLASS (FRONT VIEW). 66

FIGURE 33. POLYIMIDE FIBERGLASS (BACK VIEW). 66

FIGURE 34. POLYIMIDE FIBERGLASS RUN 12. 71

FIGURE 35. POLYIMIDE FIBERGLASS RUN 15. 71

FIGURE 36. POLYIMIDE FIBERGLASS RUN 8. 72

FIGURE 37. POLYIMIDE FIBERGLASS RUN 5. 72

FIGURE 38. POLYIMIDE FIBERGLASS RUN 18. 73

FIGURE 39. POLYIMIDE FIBERGLASS RUN 20. 73

FIGURE 40. POLYIMIDE FIBERGLASS EXIT HOLE RUN 18. 74

FIGURE 41. POLYIMIDE FIBERGLASS EXIT HOLE RUN 20. 74

FIGURE 42. F2 EPOXY SAMPLE. 76

FIGURE 43. CLOSE-UP OF DAMAGE OF F2 EPOXY RUN 1. 78

FIGURE 44. CLOSE-UP OF DAMAGE OF F2 EPOXY RUN 2. 78

FIGURE 45. CLOSE-UP OF DAMAGE TO F2 EPOXY RUN 3. 79

FIGURE 46. F2 EPOXY (FRONT VIEW). 81

FIGURE 47. F2 EPOXY (SIDE VIEW). 81

FIGURE 48. F2 EPOXY (BACK VIEW). 82

FIGURE 49. CLOSE-UP OF DAMAGE TO F2 EPOXY RUN 7. 84

FIGURE 50. CLOSE-UP OF DAMAGE TO F2 EPOXY RUN 5. 84

FIGURE 51. CLOSE-UP OF DAMAGE TO F2 EPOXY RUN 16. 85

FIGURE 52. CLOSE-UP OF DAMAGE TO F2 EPOXY RUN 20. 85

FIGURE 53. CLOSE-UP TO DAMAGE OF F2 EPOXY RUN 12. 86

FIGURE 54. CLOSE-UP DAMAGE TO F2 EPOXY RUN 15. 86

LIST OF TABLES

TABLE 1. COMPARISON OF TJNAF FEL WITH A WEAPON FEL. 17

TABLE 2. IRRADIATION OF PHENOLIC RESIN SAMPLE 1 30

TABLE 3. IRRADIATION OF PHENOLIC RESIN SAMPLE 2 34

TABLE 4. RECESSION RATES OF PHENOLIC RESIN SAMPLES 1 AND 2. 36

TABLE 5. IRRADIATION OF PYROCERAM SAMPLE 1. 38

TABLE 6. IRRADIATION OF PYROCERAM SAMPLE 2. 40

TABLE 7. IRRADIATION RESULTS OF SLIP-CAST FUSED SILICA. 42

TABLE 8. IRRADIATION DATA OF SLIP-CAST FUSED SILICA SAMPLE 1. 50

TABLE 9. IRRADIATION DATA OF SLIP-CAST FUSED SILICA SAMPLE 2. 52

TABLE 10. IRRADIATION DATA OF SLIP-CAST FUSED SILICA SAMPLE 3. 56

TABLE 11. IRRADIATION DATA OF MARCH 1999 SLIP CAST FUSED SILICA SAMPLE 3. 60

TABLE 12. IRRADIATION OF POLYIMIDE FIBERGLASS. 63

TABLE 13. POLYIMIDE FIBERGLASS IRRADIATION RESULTS. 68

TABLE 14. IRRADIATION OF POLYIMIDE FIBERGLASS, MARCH 1999 69

TABLE 15. IRRADIATION OF F2 EPOXY. 77

TABLE 16. F2 EPOXY IRRADIATIONS RESULTS. 83

TABLE 17. IRRADIATION RESULTS OF MARCH 1999 EXPERIMENT ON F2 EPOXY. 87

I. INTRODUCTION

There is no longer another navy in the world to pose a threat for the U.S. Navy on the high seas. The primary focus of concern has shifted to the littorals with emphasis on power projection ashore from the sea, and support of the land forces. This new operating environment has revealed several new vulnerabilities of U.S. Naval forces. These vulnerabilities were not anticipated when current ship's systems were being designed and built. One of the primary vulnerabilities of U.S. Navy ships is attack by high-speed anti-ship missiles, and operating in the littoral environment exacerbates this vulnerability.

A. LASER WEAPONS

One promising solution to reduce this vulnerability is to use a high-energy laser with a beam focused on the incoming missile to destroy it at long range. Such a laser would have to emit enormous power, but be small enough to fit on a ship. It would also be required to operate at a wavelength that propagates well through the atmosphere ensuring that range does not suffer, and be required to operate without producing dangerous byproducts that cannot be disposed of at sea.

The free electron laser (FEL) is a laser that appears to have the potential to satisfy these requirements. The FEL, which can be designed to operate over a wide range of

wavelengths, is the only laser capable of adapting to changing environmental conditions.

It has been demonstrated that the FEL can be tuned over a range of wavelengths up to about a factor of ten. Other lasers such as chemical lasers, gas discharge lasers, and excimer lasers, are confined to a specific wavelength by their generation mechanism.

This report describes material damage experiments conducted at the Thomas Jefferson National Accelerator Facility (TJNAF) using an FEL. It consolidates results from material damage studies and contains the work reported in six thesis conducted by students at the Naval Postgraduate School [Refs: 1 through 6]. They are the first experimental tests that study the damage on materials of interest to directed energy, from a short-pulsed laser at a high repetition rate with a few hundred watts of average power. One of the primary purposes of these experiments was to develop scaling rules that verify the conditions where small-scale damage experiments can represent the damage from a large, MW-class weapon.

II. LASER MATTER INTERACTION THEORY AND PREDICTIONS

The interaction between high-power lasers and matter is a complicated issue. The laser beam has the unique ability to deliver very high power per unit area. When high power laser radiation falls on a target, the part of the beam that is absorbed begins to heat the target surface very rapidly to its melting temperature. This melting process then penetrates progressively into the material. Many physical processes govern the damage caused to the material by the laser power including power absorption, power reflection, heat conduction, and heat diffusion. Furthermore, a large number of parameters play a major role in these processes such as material density and heat capacity, as well as the irradiation wavelength, power density, peak power, and pulse characteristics.

A good knowledge of these mechanisms helps one understand the capabilities and limitations of the laser beam, allowing complete control of the damage caused by the laser. Controlled damage has many industrial applications such as the creation of thin coatings, electronic component fabrication, very precise drilling, cutting, etc.

However, when using a high power laser beam as a weapon to shoot down incoming missiles, precision and symmetry of the damage induced are not the issues. The goal for a laser

weapon is to cause the maximum possible damage as quickly as possible with the power available.

A. REQUIRED POWER TO DESTROY TARGET

In addition to determining scaling rules, a second major reason behind the experiments discussed in this report was to determine just how much power from a short-pulse FEL is needed to destroy a missile in the few seconds allowed for engagement.

One estimate can be made by assuming that the laser burns through the material by breaking the cohesive bonds of individual atoms, and removing them one at a time. In actuality the matter would most likely disintegrate in segments of atoms rather than one atom at a time, thus reducing the number of bonds that actually have to be broken. However, some power may be wasted in heating atoms beyond the temperature needed to remove them.

One of the materials irradiated during the experiments was aluminum. The binding energy of aluminum is approximately 3.5 eV/atom [Ref. 7. pg. 74]. If the casing is assumed to be made of 3 layers of material, each about 1 cm thick, and the laser spot size on the target is 100 cm^2, the volume of material to be removed is approximately 300 cm^3. The atomic spacing for aluminum is approximately 2.5 angstroms [Ref. 7. Pg. 98], or 2.5×10^{-8} cm. This estimates the total number of atoms to be removed as

$$\frac{300\text{cm}^3}{\left(2.5 * 10^{-8}\text{cm}\right)^3} \approx 2 * 10^{25} \quad \text{atoms.} \tag{1.}$$

The total energy required is therefore

$$\begin{aligned} E_o &= \left(2 * 10^{25}\text{atoms}\right)\left(3.4\text{eV / atom}\right)\left(1.6 * 10^{-19}\text{J / eV}\right) \\ &\approx 10\ \text{MJ} \end{aligned} \tag{2.}$$

To deliver 10 MJ of energy in 3 to 4 seconds requires approximately 3 MW at the target, assuming all the energy is absorbed. Three MW divided over 100 cm^2 gives a required intensity of $\Phi = 30$ kW/cm^2. The actual required intensity level would be determined by the amount of reflected energy. Assuming a 50% loss to reflection puts the required intensity level at $\Phi = 60$ kW/cm^2.

A second method to estimate the required intensity is to determine the amount of energy needed to bring the material to vaporization temperature. Assuming that the energy is delivered at a rate much greater than the heat loss through diffusion, the required energy can be determined from [REF. 8. pg 167] .

$$E_o = \rho d \left(C[T_m - T_o] + \Delta H_m + C[T_v - T_m] + \Delta H_v\right) \tag{3.}$$

where E_o is the required flux density, $\rho =$ density, d = thickness of material to be burned through, C = Specific

Heat, T_m = melting temperature, T_o = ambient temperature, T_v = vaporization temperature, ΔH_m = latent heat of melting, and ΔH_v = latent heat of vaporization.

For aluminum the specific values are: $\rho = 2700$ kg/m^3, d = 3 cm, C = 896 J/kg-K, T_m = 855 K, T_o = 300 K, T_v =2750 K, $\Delta H_m = 4 * 10^5$ J/kg, and $\Delta H_v = 10.8 * 10^6$ J/kg. Using these values in equation (3.) gives a required energy of

$$E_o \approx 1 \text{ GJ} / \text{m}^2 \qquad (4.)$$

or

$$E_o \approx 10^5 \text{J} / \text{cm}^2 . \qquad (5.)$$

This much energy delivered over a 3 second engagement requires an intensity approximately $\Phi = 35$ kW/cm^2, for a total beam power of approximately 3.5 MW to place a 100 cm^2 spot on the target. This is consistent with the 3 MW requirement developed using the first approximation method.

A second material irradiated during the experiments is Slip-Cast Fused Silica, a furnace tile like material. The specific parameters for this material are $\rho = 2200$ kg/m^3, d = 9 mm, C = 920 J/kg-K, T_m = 1980 K, T_0 = 300 K, T_v = 2200 K, $\Delta H_m = 1.5 \times 10^6$ J/kg, $\Delta H_v = 2.2 \times 10^6$ J/kg. Using these numbers in equation (3.) shows that 11 kJ/cm^2, or about 3

kW/cm^2 over a 3 to 4 second irradiation should be enough energy to burn through the material. This is nine times smaller than that derived for aluminum because the thickness of the Slip-Cast Fused Silica used here was 1/3 of the thickness of the aluminum used in the example. Using the same 3cm thickness for Slip-Cast Fused Silica gives a total required flux of 35 kJ/cm^2, or an required intensity of approximately $\Phi = 10$ kW/cm^2 for a 3 to 4 second engagement.

These estimatations give an order of magnitude approximation of the energy that is actually needed to melt through the missile. As reported later in this document, an intensity level of 10 kW/cm^2 was enough to melt through an aluminum sample that was cut to the correct size to control the thermal diffusion. However, when a sample of Slip-Cast Fused Silica was irradiated at the same intensity level, burn through was only achieved after an extended time of almost two minutes. A possible explanation will be discussed in Chapter V, Section B.3.a.

Experiments conducted in the 1970's and 1980's in conjunction with the MIRACL program indicate that an energy flux or power density, Φ = 10 kW/cm^2 is needed to destroy a missile with a dwell time of a few seconds. For this reason most of the experiments discussed later in the report were conducted at an intensity level of approximately 10 kW/cm^2.

B. SCALING LAWS AND MINIMAL SPOT SIZE

Laser damage to material has been studied for many years. Several Department of Defense and agencies have used various lasers to determine damage to different materials. Laser damage to material is not a new subject, but using a FEL to incur the damage is new.

Since there is no MW-class FEL to perform full-scale experiments, scaling is the only way to determine the effectiveness of a FEL weapon. As mentioned in the previous section, a power density Φ = 10 kW/cm^2 over a spot size A ≈ 100 cm^2 is required to destroy a missile with a dwell time of a few seconds. Scaling laws would allow predictions of large area damage from small area experiments. To achieve a power density of Φ = 10 kW/cm^2, a 100 W FEL must use a spot size of 1 mm^2, while a 1 kW laser uses a spot size of 10 mm^2.

Scaling of the laser damage will only work, however, if the thermal diffusion is independent of spot size. Schriempf calculates the thermal diffusion length to be

$$D = 2\sqrt{\kappa t} \tag{6.}$$

where $\kappa = \frac{K}{\rho c}$ is the thermal diffusivity and

$$t = \frac{\pi K^2 \Delta T^2}{4\Phi_0^2 \kappa}, \tag{7.}$$

where t is the time required to bring the material from ambient temperature to melting temperature. [Ref. 9] The thermal diffusion length D represents the distance required for T to drop to $1/e$ times its initial value. In the semi-infinite approximation used by Schriempf, radial heat flow is ignored. In order for this to be valid, the spot size must be much larger than D, or the target diameter $d \leq D$. If these conditions are not met, heat will diffuse outside of the laser spot and the spot will not be heated effectively.

C. PULSE TRAIN

The pulse train of an FEL is different from other lasers. FELs produce short, powerful pulses with a rapid repetition rate.

Short pulsed lasers, microseconds or shorter, the peak power increases and may cause new effects beyond thermal heating. Due to the higher peak laser energy, there can be rapid vaporization at the target surface, so that the recoil from the vapor blowoff forms a strong pressure wave. The peak of the pressure wave, or impulse, induces a shock front, while the rear of the wave induces a rarefaction wave. The shock front reflects when it reaches a free surface at the rear of the material. The super position of the reflected and incident waves results in stress at the

free surface, which can exceed the material strength causing catastrophic damage to the material. [Ref. 10]

The TJNAF FEL has a pulse length of τ = 0.4 ps and a repetition period of T = 27 ns illustrated in Figure 1. The duty cycle D_u is the fraction of time the laser is actually irradiating the target,

$$D_u = \frac{\tau}{T} = \frac{4 \times 10^{-13}\text{s}}{2.7 \times 10^{-8}\text{s}} = 1.5 \times 10^{-5}. \qquad (8.)$$

The peak power in each micropulse $\hat{P}$ is

$$\hat{P} = \frac{\overline{P}}{D_u} = \frac{1700\text{W}}{1.5 \times 10^{5}} = 110\text{MW}, \qquad (9.)$$

where $\overline{P}$ is the current average power of 1700 W for the Thomas Jefferson National Accelerator Facility (TJNAF) FEL.

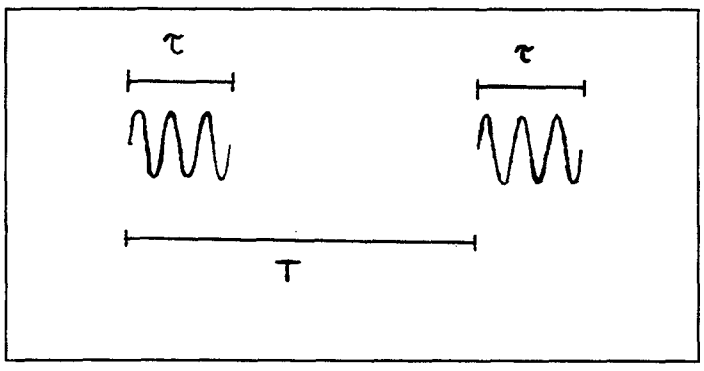

Figure 1. FEL Pulse Format.

Comparing the TJNAF FEL to another short pulse laser is instructive. The Lawrence Livermore National Labs (LLNL) 1.053 μm Ti:sapphire CPA system has a pulse length $\tau = 0.4$ ps, but a pulse repetition rate of only 10 Hz, so the period is $T = 0.1$ s, and the peak power is $\hat{P} = 2.5\text{TW}$ [Ref. 11]. The duty factor is

$$D_u = \frac{4 \times 10^{-13}\text{s}}{0.1\text{s}} = 4 \times 10^{-12}, \tag{10.}$$

so that the average power is

$$\overline{P} = \left(2.5 \times 10^{12}\text{W}\right)\left(4 \times 10^{-12}\right) = 10\text{W}. \tag{11.}$$

Note that the LLNL laser has a much higher peak power than the TJNAF FEL, but the TJNAF FEL has more than one hundred times the average power because of its high duty cycle. The experiments detailed in the following section were conducted to study the effects of the unique FEL pulse format in laser-matter interaction on small samples.

D. ULTRA-SHORT PULSES

In recent years, new laser capabilities have allowed damage research with ultra-short laser pulses, from picosecond to femtoseconds. Ultra-short laser pulse lengths deliver energy to a metal at such a fast rate that the metal

lattice cannot respond, but the electrons can [Ref. 12]. The electrons rapidly increase in temperature so that the difference between electron and lattice temperatures can be as much as a few thousand degrees. Eventually, electron-phonon interactions distribute the excess energy between the electrons and the lattice in a time equal to a few phonon oscillations periods, a few to tens of picoseconds [Ref. 13].

A theory developed to describe the effect of pulse-duration on optical damage to metals argues that with ultra-short pulses, the electrons penetrate the material to a certain heat deposition depth before coupling to the lattice [Ref. 14]. For pulses shorter than the lattice relaxation time, the heat-deposition depth is relatively large and the resulting damage threshold fluence, E_{th}, is independent of pulse duration. For pulse lengths longer than a critical time, τ_c, which is larger than the relaxation time by a factor of C/C_eT_m where C is the material heat capacity, C_e is the electron heat capacity, and T_m is the melting temperature, the diffusion of energy to the lattice becomes important. In this case, E_{th} will scale as the square root of the pulse length, $\tau_p^{1/2}$ [Refs. 14 to 16]. For pulses shorter than about 500 picoseconds, E_{th} becomes independent of pulse length. Experiments show that there may be as much as a factor of 10 advantage when using shorter picosecond pulses over the larger 100 nanosecond pulses. [Ref. 14]

Research has also examined the threshold for ultra-short pulses damaging dielectrics [Refs. 11, 17] The same trend as was observed with metals was observed in the dielectrics. For the longer pulses, the damage threshold decreases with decreasing pulse length as $\tau_p^{1/2}$ and does not depend on pulse length for very short, picosecond pulses. The critical pulse length, τ_c, for the transition was hundreds of picoseconds for metals, but is only a few picoseconds for dielectrics. As with metals, it appears that there may be as much as a factor of ten advantage when using shorter picosecond pulses compared to longer nanosecond pulses.

From these earlier studies, it may be inferred that there is a possibility of decreasing the fluence required to cause damage to a material with ultra-short picosecond pulses compared to CW or short nanosecond pulses. If it is true, then it may be possible that the energy required to damage an in-bound missile could be reduced. The advantage could decrease the size of the FEL required on board ship, decrease the possibility of thermal blooming, and decrease the dwell time on target.

For the experiments conducted on March 12 and March 23, 1999, the only parameter changed was the pulse repetition frequency, which caused the pulses used in the later experiments to have twice the fluence per pulse as the pulses on March 12th. The burn through rate for the

experiments of March 23 was faster, and it is postulated that the increase is because the higher fluence pulses of 0.12 J/cm^2 of enery. This is slightly greater than the ablation threshold for picosecond pulses on metals, and some ablation of the material may have taken place. [Ref. 18] However, the fluence level was not high enough to create the impulse damage and pressure waves discussed in the paragraphs above.

III. TJNAF FACILITY

A. TJNAF FEL

The most powerful FEL ever operated is at the Thomas Jefferson National Accelerator Facility (TJNAF), located in Newport News, Virginia. It is an U.S. Department of Energy facility that is operated and maintained by the Southeastern Universities Research Association (SURA), Incorporated. The TJNAF FEL first lazed on June 15, 1998, with a pulsed electron beam. Two days later, it increased power output to 155 Watts of continuous wave power. By July 29, 1998, TJNAF increased the laser output power to 311 Watts, a 28-fold increase over any other FEL. On March 11, 1999, TJNAF increased the output power to 710 Watts, using a recirculated beam. In July 1999, the laser operated continuously at 1720 Watts of average power. Near term modifications now in the planning stage will boost the power to 10 kW. With additional research and development, a MegaWatt Class FEL could soon be realized.

Figure 2 is a diagram of the current FEL. Figure 3 shows the modifications that will boost the output power to allow for a 10 kW infrared wavelength laser or a 1 kW ultraviolet wavelength laser. Industrial applications are planned for the ultraviolet wavelengths.

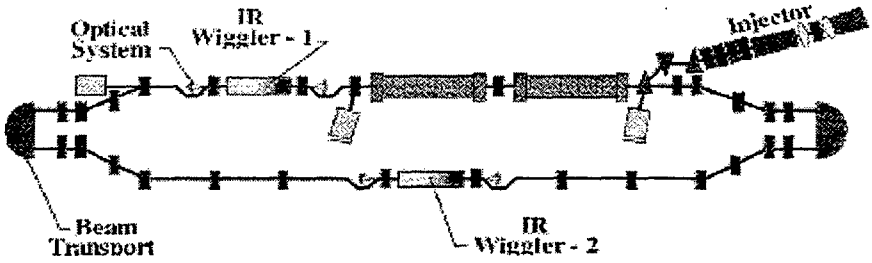

Figure 2. Current FEL Configuration.

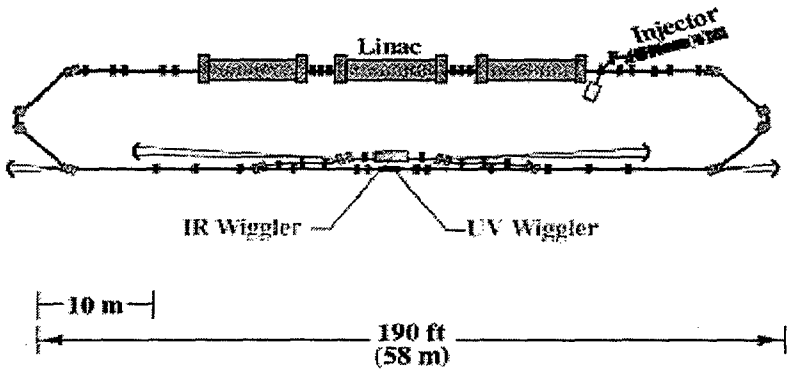

Figure 3. Upgraded FEL Configuration.

Table 1 shows the parameters of the TJNAF FEL and compares them to the requirements for a proposed shipboard anti-missile defense weapon [Ref. 19].

Table 1. Comparison of TJNAF FEL with a Weapon FEL.

Parameter	TJNAF FEL	Weapon FEL
Average Power	$\overline{P}$ = 1.7 kW	$\overline{P}$ = 1 MW
Average Current	$\overline{I}$ = 5 mA	$\overline{I}$ = 900 mA
Electron Energy	γmc^2 = 48 MeV	γmc^2 = 100 MeV
Electron Charge/Bunch	I_e/c = 60 pC	I_e/c = 1800 pC
Peak Current	$\hat{I}$ = 60 A	$\hat{I}$ = 600 A
Electron Beam Radius	r_b = 100 μm	r_b = 300 μm
Pulse Length	τ = 0.4 ps	τ = 3 ps
Pulse Repetition Rate	*PRR* = 18.7/37.4/74.85 MHz	*PRR* = 500 MHz
Output Coupling	10%	10%
Resonator Cavity Losses	$\mathcal{Q}$ = <0.5% / pass	$\mathcal{Q}$ = <0.5% / pass
Optical Wavelength	λ = 3-6 μm	λ = 1 μm

The significant differences are increases in the peak current by a factor of 10, the repetition rate by a factor of 7, the electron beam energy by a factor of 2, and the pulse length by a factor of 7.

B. USER LAB

Once the FEL beam was produced, it was transferred to several user laboratories for various applications. The beam was transferred via a low loss optical path. All laser

damage experiments referred to in this report were conducted in user laboratory number one. Various TJNAF personnel operated the equipment to conduct the experiments including Michelle Shinn, Steve Benson, Richard Evans, B. Yunn, K. Jordan, J. Gubeli, and George Neil. Figure 4 is a picture of the optical bench setup used for experiments. The setup included a focusing calcium fluoride lens, a sample holder, an iris and a power meter. In Figure 4 the number 1 corresponds to the lens. The sample holder is not shown in the picture, but the line numbered 2 denotes its position on the bench set up. The line numbered 3 is the focus of the lens, object number 1. Object 4 is an iris. The power meter will be shown in a later picture. Two video cameras were setup to record the experiments, one in front of the sample holder and one behind.

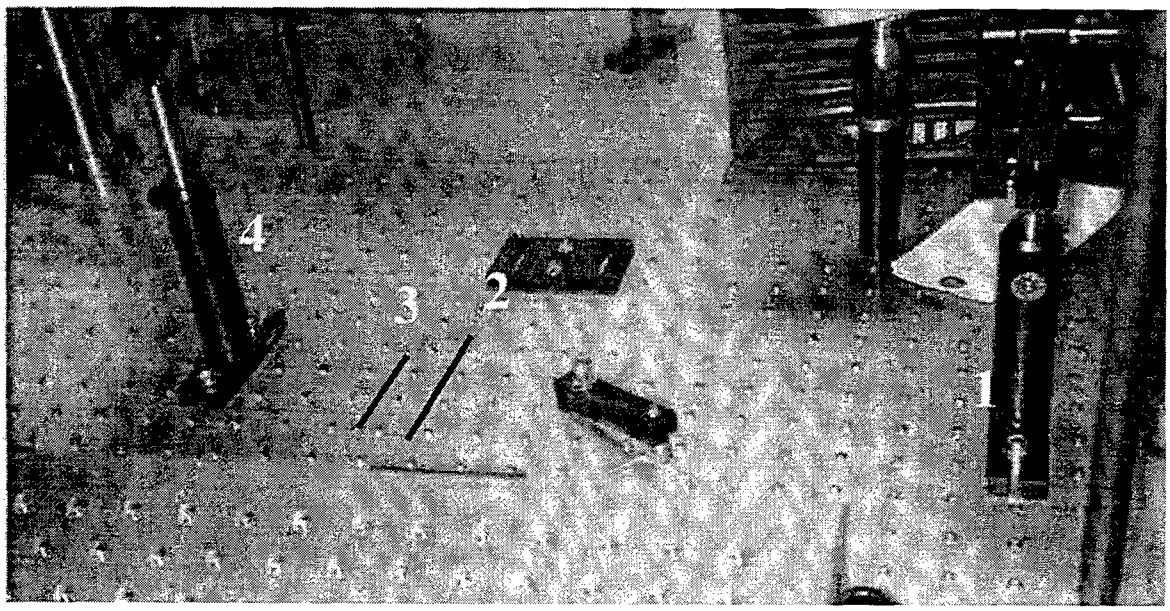

Figure 4. Optical Bench.

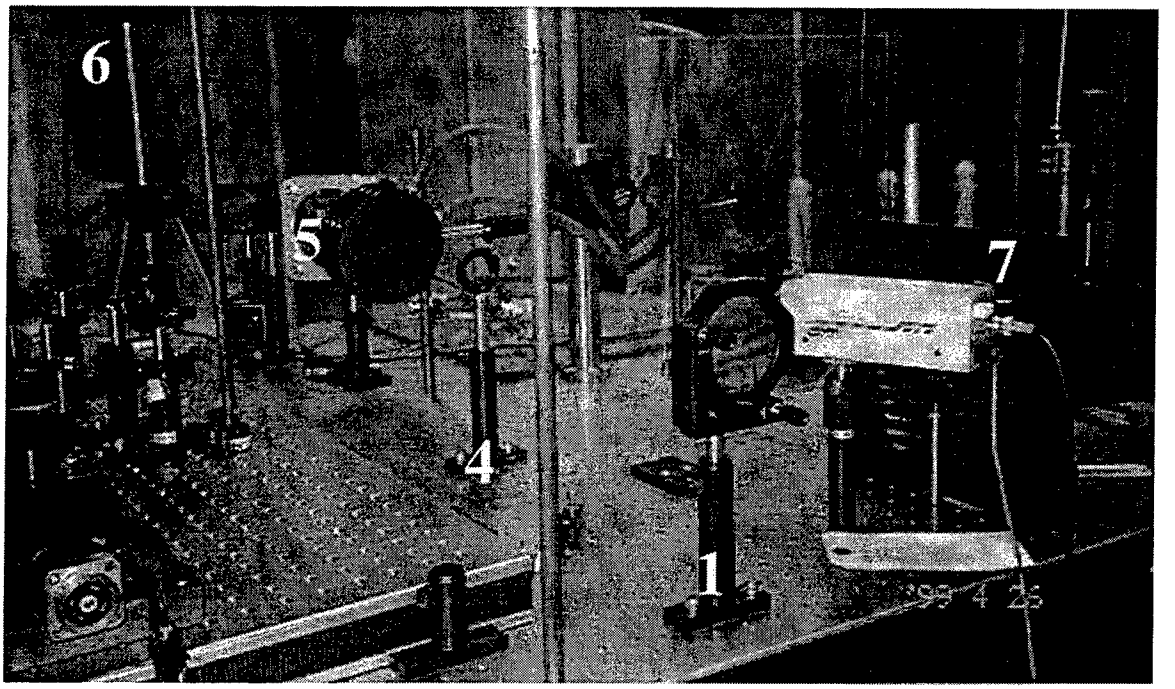

Figure 5. Front view of optical bench.

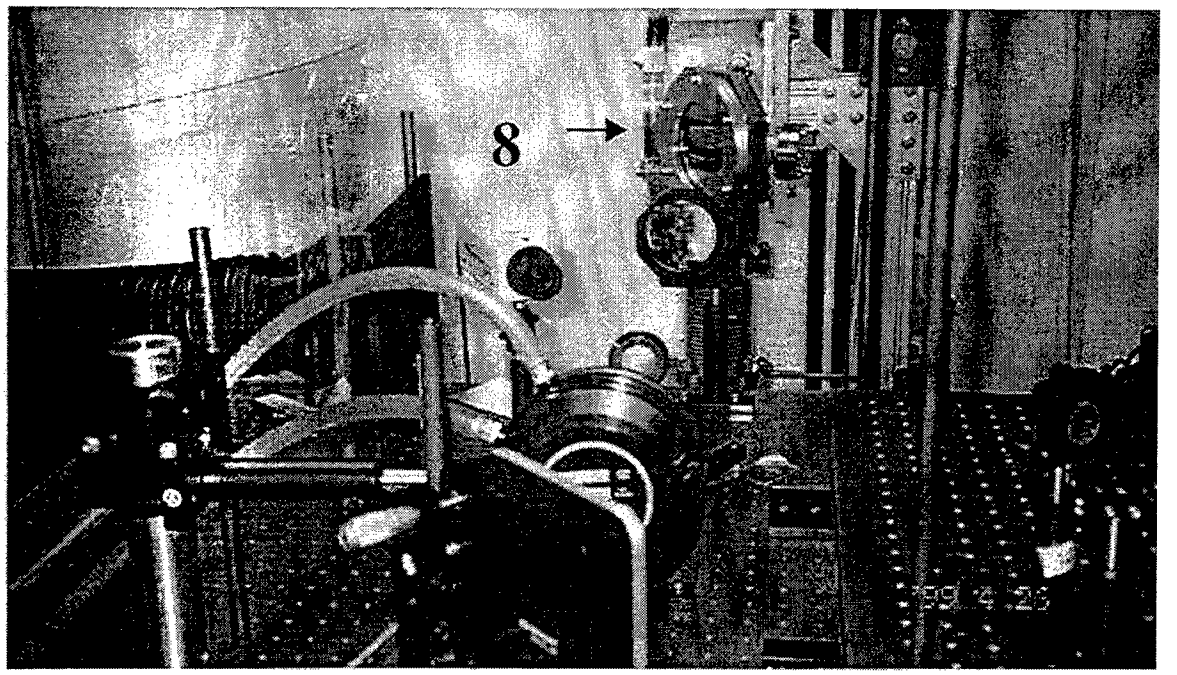

Figure 6. Rear view of optical bench.

Figure 5 is the front view of the optical bench. The number 1 indicates to the lens as before. The number 5 shows the power meter's location. Numbers 6 and 7 show the positions of the back and front video cameras, respectively.

Figure 6 is a rear view of the optical bench. The number 8 correlates to the output of the transfer equipment used to transfer the FEL beam to the user laboratory.

IV. MATERIALS

A. MATERIALS USED IN EXPERIMENTS

In addition to the aluminum samples tested in these experiments, five other materials were also used. The materials chosen were either actual missile nose cone materials, or materials that were very similar to missile nose cones. The materials are [Refs. 20, 21]:

1. Phenolic Resin

   Radome material from a Standard ARM Missile.

2. Pyroceram

   A furnace coating type material used in SM-1 and SM-2 missile radomes.

3. Slip-Cast Fused Silica

   Commercially available furnace material. Similar to material used as a radome for Patriot missile system.

4. Polyimide Fiberglass

   A high temperature fiberglass used on supersonic missile radomes.

5. F2 Epoxy

   Five plies of fiberglass cloth with an epoxy binder. This type of material is used in the Soviet STYX type missiles.

B. THERMAL DIFFUSION CALCULATIONS

A calculation of the thermal diffusion length associated with heating the sample to melting temperature was performed for a small piece of aluminum (Al-6061). This material had values density ρ = 2700 Kg/m^3, specific heat C = 896 J/Kg-K, thermal conductivity K = 180 W/m-K, thermal diffusivity κ = 7.44 x 10^{-5} m^2/s, T_m= 855K, Φ_0 = 10^8 W/m^2 and

$$D = 2\sqrt{\kappa t}, \tag{12.}$$

$$t = \frac{\pi K^2 \Delta T^2}{4\Phi_0^2 \kappa}, \tag{13.}$$

where t = 0.01s is the time required to bring the material from ambient temperature to melting temperature and $\Delta T \approx$ 550K is the temperature change. The result for Al-6061 is D = 2mm. In order to melt through an aluminum sample, the laser spot must have an area greater than π(2 mm)$^2 \approx$ 10 mm^2. Alternately, the target itself can be made small with d $\approx$ D. These calculations were experimentally verified with samples of Al-6061. Using a laser spot size of 1 mm^2 (much smaller than the required 10mm^2), a sample with 1 cm diameter was irradiated with no melting after several

minutes. Other samples with a diameter of 2mm (very close to the laser spot size itself) were melted in a few seconds.

Another target irradiated was Slip-cast Fused Silica (SiO_2). A calculation of the thermal diffusion length associated with heating the sample to its melting temperature of 1980K was performed using values ρ = 2200 Kg/m^3, C = 920 J/Kg-K, K = 1.26 W/m-K, $\kappa = 5 \times 10^{-7}\ m^2/s$, T_m= 1980K, $\Phi_0 = 10^8\ W/m^2$. Since this material has a low thermal diffusivity, its thermal diffusion length is also small, D = 0.02mm. Therefore, with the insulating material, fused silica, the scaled laser spot must have an area greater than $\pi(0.02\ mm)^2 = 0.001\ mm^2$, which was attained with the 1 mm^2 and larger beams used at TJNAF.

V. MATERIAL DAMAGE EXPERIMENTS

A. EXPERIMENTAL PROCEDURES

1. March 1999

Samples of all five materials were irradiated by a laser beam of wavelength $\lambda = 4.825$ μm through a calcium fluoride lens with a focal length of 300 mm. Two pulse repetition frequencies (PRF) were used; 74.85 MHz for the Phenolic Resin sample and 37.42 MHz for all other samples. The average power recorded on the power meter in the user lab read 100 to 103 W with an error of ±5 W. Since a lens focused the beam, the beam area decreased with distance along the direction of propagation to a minimum waist radius of $w_0 = 80$ μm at the focal point. *PARAXIA*, a beam propagation code, was used to model the beam diffraction and find the target position giving the desired intensity of 10 kW/cm^2 [Ref. 22]. Figure 7 shows a graph of irradiance versus distance from the focal point, with the negative numbers indicating positions in front of the focus.

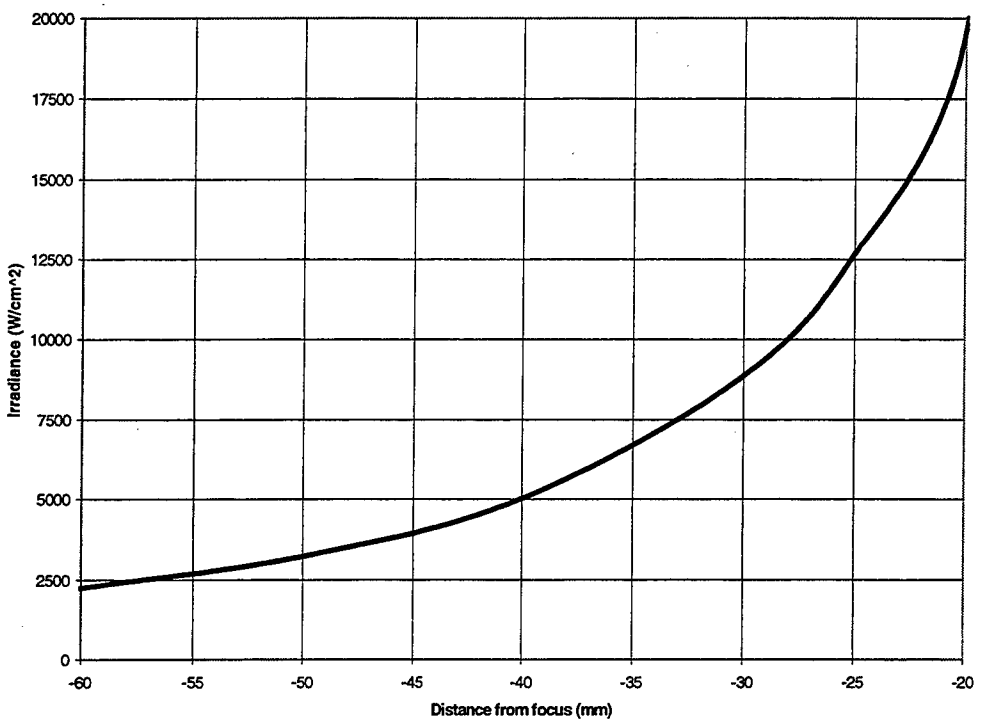

Figure 7. Irradiance vs. Distance from Focal Point.

An irradiance of 10 kW/cm^2 occurred when the sample was placed between 25 mm to 30 mm in front of the focal point. The samples were actually placed 26 mm in front of the focus. Note that as the laser burns into a sample at some depth, the intensity actually changes by a small amount due to diffraction. The burn-through time was determined by observing a signal on a power meter placed behind the samples, and by watching for the presence of coherent harmonics in the visible spectrum on an iris placed approximately 15 cm behind the samples.

2. August 1999

In the August 1999 experiments, three of the original five materials were used: Slip-Cast Fused Silica, Polyimide Fiberglass, and F2-Epoxy. Airflow was also added to the experiments to determine if it would have any effect on the burn through rates.

Two samples of Slip-Cast Fused Silica were irradiated through a calcium fluoride lens with a measured back focal length of 137.6 mm at 3 μm. The laser beam wavelength was λ=3.10 μm, the pulse repetition frequency (PRF) was 18.7 MHz, and the power meter in the optics control room indicated a power of 105±5 W. The samples were placed 20.7 cm from the back surface of the lens. At this position the calculated waist radius of the beam was 0.25 cm, with a corresponding average intensity of 490 W/cm^2. Three irradiations with no airflow were done, then the air was turned on and three more irradiations were done. The air was blowing across the front face of the sample. An Oregon Scientific anemometer was used, which indicated a airflow speed of 60 mph. The irradiation exposure time was 5 sec.

After finishing the above irradiations a new sample was used. The sample was moved in a new position in order to achieve a beam waist radius of 0.087 cm, which yields to an average intensity of 10 kW/cm^2. The same irradiation schedule was followed. The irradiation exposure time was again 5 sec. [Ref. 23]

For the Polyimide Fiberglass and the F2-Epoxy, each sample was irradiated with a FEL beam of wavelength 3.1 μm, pulse repetition frequency 18.7 MHz and average power 100W±5W. The Polyimide Fiberglass was irradiated first, followed by the F2-Epoxy. Measurements were made with samples placed downstream of a calcium fluoride lens with a measured back focal length of 137.6 mm for 3 μm wavelengths. A camera was set up to observe the front and back surface of the samples.

Two sets of three irradiations were first made. The average intensity was 490 W/cm^2, which was achieved by focusing the beam to a spot of 0.25 cm radius. Three identical irradiations were made initially with no airflow, and then three again with a airflow speed of 60 mph across the front face of the samples. Then, adjusting the beam radius to 0.087 cm, the intensity was set to 10 kW/cm^2 and the same set of measurements was repeated.

3. March 2000

In the March 2000 experiments, the same three materials that were used in the August 1999 experiments were again irradiated. The goal of these measurements was to maintain the average intensity of 10 kW/cm^2 but use higher laser power, in order to achieve a larger spot size.

The Slip-Cast Fused Silica sample was irradiated through a calcium fluoride lens with a measured back focal length of 235.7 mm at 3 μm. The laser beam wavelength was λ=3.10 μm, the pulse repetition frequency (PRF) was 37.4 MHz, and the power meter in the optics control room indicated a power of 500±10 W. The samples were placed 217.0 mm from the back surface of the lens. At this position the calculated waist radius of the beam was 0.12 cm, with a corresponding average intensity of 10 kW/cm^2. One irradiation with no airflow was done, then the air was turned on, and one more irradiation was done next to the first one. The air was blowing across the front face of the sample. An Oregon Scientific anemometer was used, which indicated a airflow speed of 83-86 mph. The irradiation exposure time was 5 sec.

The Polyimide Fiberglass and F2-Epoxy samples were again irradiated 6 times (2 sets of 3 irradiations) with a FEL beam of wavelength λ = 3.1 μm, pulse repetition frequency 37.4 MHz, and average power 500W±10W. The Polyimide Fiberglass was irradiated first, followed by the F2-Epoxy. Measurements were made with samples placed downstream of a calcium fluoride lens with a measured back focal length of 235.7 mm for 3.1 μm wavelength. A camera was set up to observe the front and back surface of the samples. Irradiations were made with 10 kW/cm^2 average intensity, which was achieved by focusing the beam to a spot

of 0.126 cm radius. Three identical irradiations were made with no airflow, and then three again with a airflow speed of 85 mph across the front face of the samples [Ref. 24].

B. EXPERIMENTAL RESULTS

1. Phenolic Resin

a) Phenolic Resin Sample 1 March 1999

Phenolic Resin sample 1 was circular with an outer diameter of 32.5 mm. There was a 7.1 mm hole in the middle of it. It varied in depth from 1.6 mm to 3.2 mm. Figure 8 is a picture of sample 1 after 3 irradiations, with the sample rotated 90° counterclockwise after each run. In Figure 8, the numbers correlate to the data in Table 2. The power meter in the lab indicated a power of 100 watts with the pulse repetition frequency of 74.85 MHz.

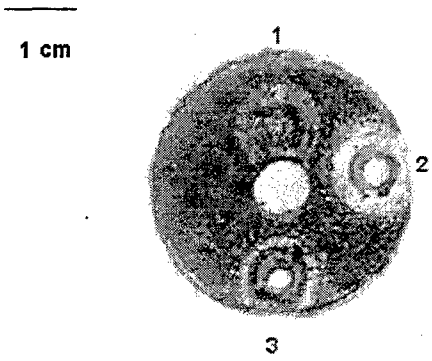

Figure 8. Phenolic Resin Sample 1.

Table 2. Irradiation of Phenolic Resin Sample 1.

Run Number	Irradiance (kW/cm^2)	Thickness (mm)	Wavelength (μm)	Exposure Time (s)	Burn Through Time (s)
1	10	1.6	4.825	3.4	N/A
2	10	2.5	4.825	11.7/26.5	7.4
3	10	3.2	4.825	13.5	7.9

The objectives of these FEL irradiations were simple: to see if the FEL would burn through the material and measure at least 50% of the incident energy on the power meter behind the sample. Run number one did not achieve burn through because of operator intervention. After initial irradiation, the rear camera showed that the sample had ignited. The FEL operators quickly stopped the

experiment only to find that the sample had slightly charred on the reverse side and had not burned through.

For run numbers two and three, the samples were irradiated for an extended period past burn through. From watching the videotape, the burn through times were approximately 7.4 seconds for run two and 7.9 seconds for run three. Neither run measured more than 50% of the incident energy on the power meter, which the operator felt was an indication that the ablative plumb was absorbing 50% of the energy [Ref. 18].

Figure 9 is a picture of run number two using a microscope and video-capturing program. Run number two is similar to run number three. The crater is not cylindrical since the back face has a slightly smaller area than the front. There is a crater lip that is built up from the damage, approximately 1mm high. Also, note the presence of the white crust, probably from the separation of the resin into its elements during heating. The white crusts and lips are also evident on the back side for runs two and three.

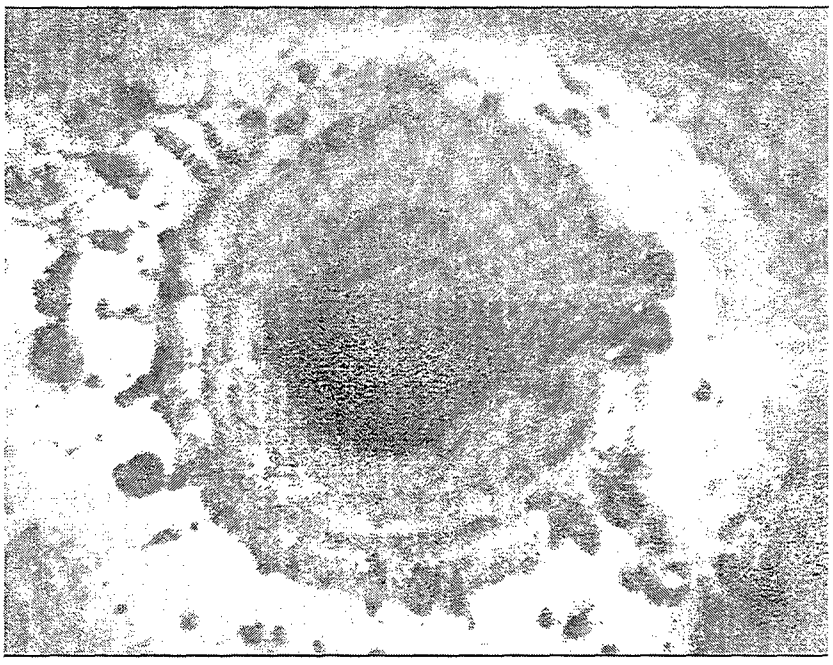

Figure 9. Phenolic Resin Sample 1, Run 2.

b) Phenolic Resin Sample 2 March 1999

Phenolic Resin sample 2 was circular with a diameter of 31.0 mm. There was a 7.1 mm hole in the middle of it. It varied in thickness from 1.5 mm to 3.8 mm. Figure 10 is a picture of sample 2 after 7 irradiations, rotated counterclockwise after each. In Figure 10, the numbers correlate to the data in Table 3. The incident power was 100 W with a pulse repetition rate was 74.85 MHz.

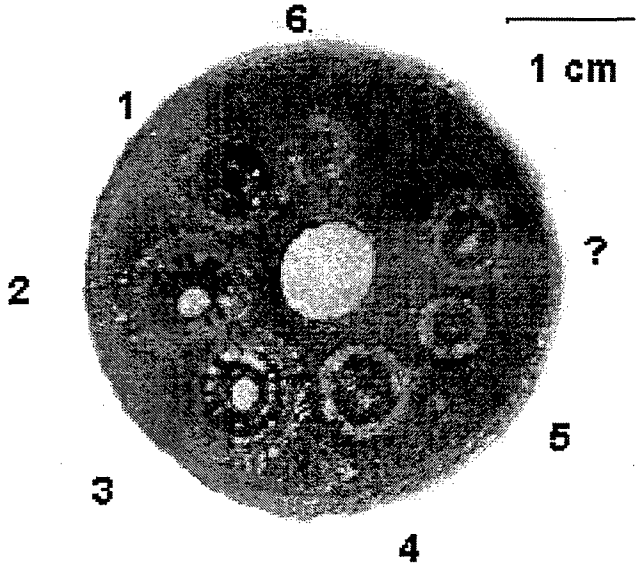

Figure 10. Phenolic Resin Sample 2.

Table 3. Irradiation of Phenolic Resin Sample 2.

Run Number	Irradiance (kW/cm^2)	Thickness (mm)	Exposure Time (s)	Burn through
1	12	3.8	1	No
2	12	2.2	2	Yes
3	12	1.7	3	Yes
4	12	1.6	0.5	No
5	680	1.5	1	Yes
6	680	3.2	2	Yes

All runs produced a lip around the entrance of the cavities ranging from 0.1 mm to 1 mm high. They also produced a white crust that must be some sort of elemental extract of the resin, probably separated during heating. Runs that did not burn through, one and four, created a crater shaped like an inverted cone with a rounded apex, probably due to the Gaussian nature of the FEL's beam. Inspection of the back side of run four, showed charring, a sign that the beam almost burned through. Runs that achieved burn through had a cylindrical crater, with the back edge slightly smaller than the front. Lips formed on the reverse side of the sample, just like the front side with the white crust around it.

Figure 11 is a picture of run number three using a microscope and video capturing program. Run number three is indicative of the runs with irradiances of 12 kW/cm^2, runs one through four. Note the crater's lip and the existence of the white crust.

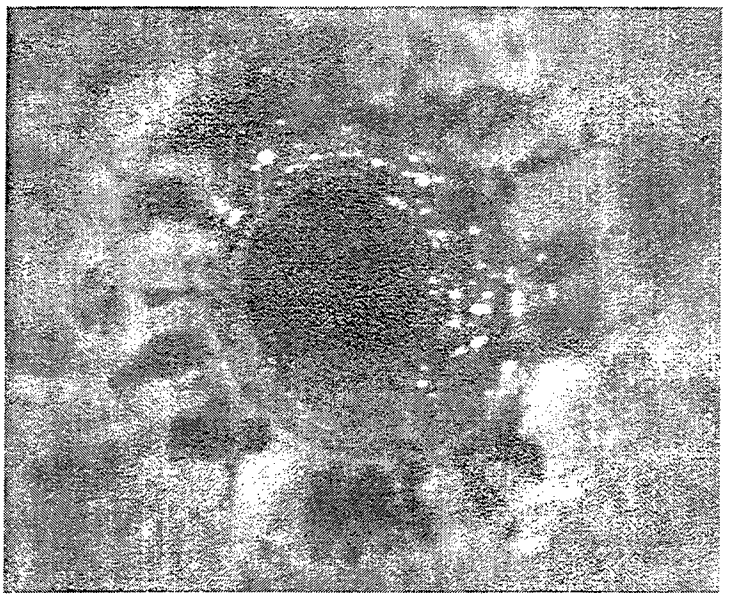

Figure 11. Phenolic Resin Sample 2, Run 3.

Figure 12 is a picture of run six. It is indicative of the damage produced by the runs with irradiances of 680 kW/cm^2, the other run was number five. Also note that due to the high irradiance, the crater is smaller in height by a factor of two or three. The beams with more power density were able to burn through the material faster producing a much smaller lip as well. Note the existence of the same

light crust but in smaller amounts.

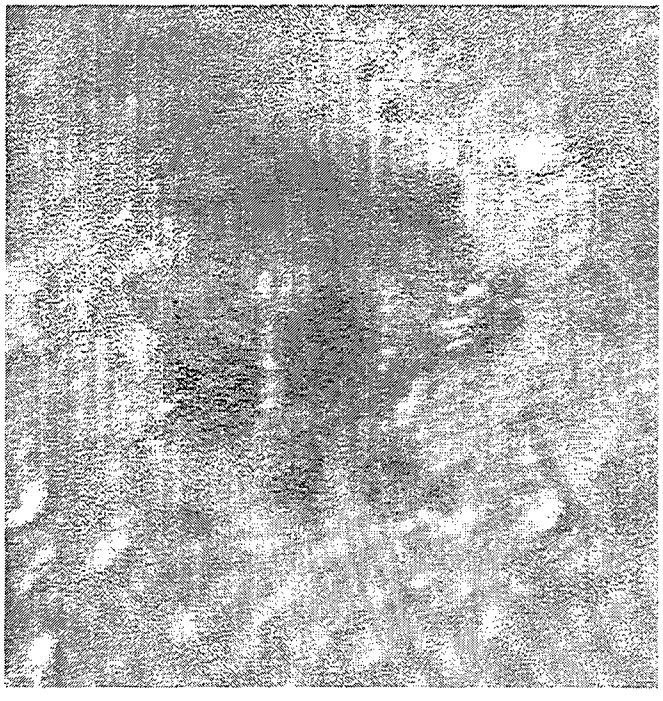

Figure 12. Phenolic Resin Sample 2, Run 6.

Table 4. Recession Rates of Phenolic Resin Samples 1 and 2.

Run Number	Depth of hole (mm)	Burn through time (s)	Penetration Rate (mm/s)
1	3.0	N/A	3.0
2	2.2	1.4	1.57
3	1.7	1.0	1.7
4	1.6	N/A	3.2
5	1.4	<0.06	>20
6	3.2	>0.06	>50

Recession rates are computed in Table 4. The burn through times were hand-timed from a video of the experiments using a stopwatch. Data from Table 4 concludes that the recession rate decreases nonlinearly as the exposure time increases. This decline is recession rate could be due to smoke and debris flying out of the crater while the beam is burning through the Phenolic material. The smoke and debris impede the laser from doing damage.

2. Pyroceram

a) Pyroceram Sample 1 March 1999

Pyroceram sample 1 was irregular in shape with an average thickness of 1.4 mm. Figure 13 is a picture of sample after 3 irradiations. In Figure 13, the numbers correlate to the data in Table 5. The power meter in the lab indicated a power of 103 W with a pulse repetition rate of 74.85 MHz, and optical wavelength of 4.83 μm.

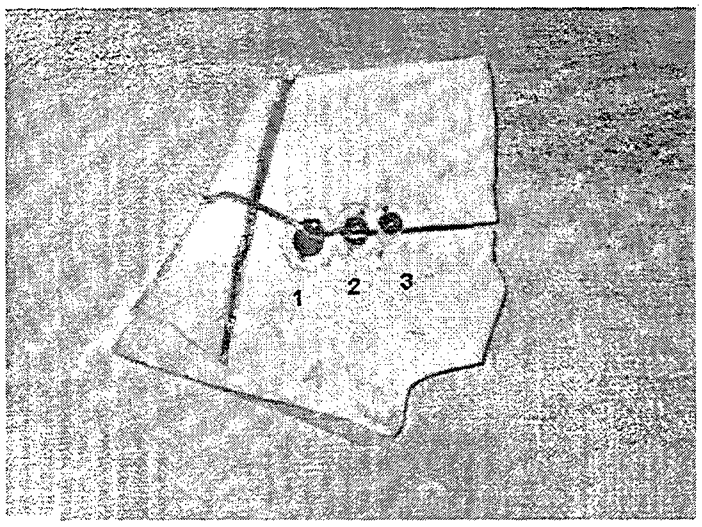

Figure 13. Pyroceram Sample 1.

Table 5. Irradiation of Pyroceram Sample 1.

Run Number	Avg. Intensity (kW/cm^2)	Exposure time (s)	Comments
1	9	2	
2	9	4	
3	9	6	Sample shattered

b) Pyroceram Sample 2 March 1999

Pyroceram sample 2 had an irregular shape with an average depth of 1.4 mm. Figure 14 is a picture of sample 2 after 3 irradiations. In Figure 14, the numbers correlate to the data in Table 6. The power meter in the lab indicated a power of 103 W with a pulse repetition rate of 74.85 MHz, and laser beam wavelength of 4.83 μm.

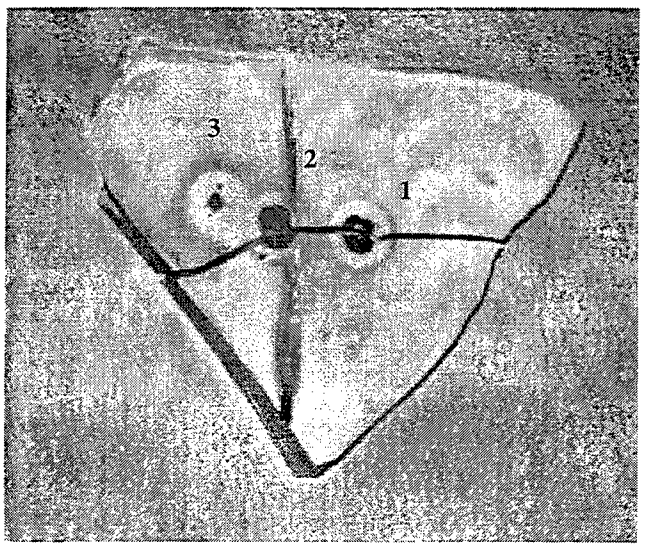

Figure 14. Pyroceram Sample 2.

Table 6. Irradiation of Pyroceram Sample 2.

Run Number	Avg. Intensity (kW/cm^2)	Exposure time (s)	Comments
1	9	7	
2	9	5	Sample shattered
3	500	11	

Each irradiation of the sample caused a spray of sparks, flying debris, and smoke. Run number three of sample 1 shattered five seconds into the six second irradiation period. Run number two of sample 2 shattered 4.5 seconds into the run. After irradiation there was molten pyroceramic material in each crater, which cooled into black glossy material as seen in Figure 13 and Figure 14. The irradiations did not produce a noticeable lip as in the Phenolic Resin tests. The runs also produced a distinct circular ring around the craters. The origin of the rings is unknown, but they may be the result of material alteration due to heating. There were no notable marks on the back of the sample. The laser beam did not burn through sample 1 or sample 2 on any run.

3. Slip-Cast Fused Silica

a) March 1999

The fused silica sample provided by NRL measured 6.9 cm x 7.4 cm and varied in thickness from 0.9 cm to 1.9 cm. The front of the sample after irradiation is shown in Figure 15.

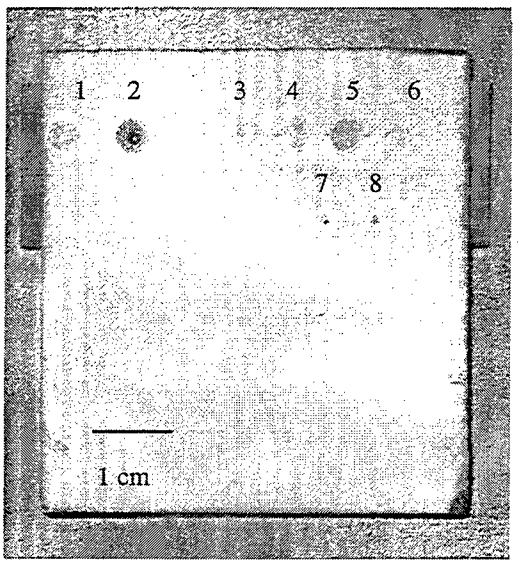

Figure 15. Slip-Cast Fused Silica Sample.

The sample was irradiated eight times and the results are summarized in Table 7.

Table 7. Irradiation Results of Slip-Cast Fused Silica.

Run Number	Average Intensity (kW/cm^2)	Exposure Time (s)	Penetration Rate (mm/s)
1	9	9	0.20
2	9	110	0.08
3	9	13	0.20
4	9	24	0.12
5	9	41	0.08
6	9	2	0.35
7	500	3	3.0
8	500	11	3.0

The irradiations were done from left to right in Figure 15. The last two runs were done with the sample at the focus of the laser beam instead of 26 mm in front, so that the beam waste radius was only 80 μm yielding an intensity of 500 kW/cm^2. The last two runs were conducted to investigate the effects of much higher power density. As shown in Figure 15, the first six runs were along the top of the sample and the last two were approximately 1 cm below. The second, seventh and eighth runs penetrated the entire 0.9-cm thickness of the Fused Silica material. Figure 16 shows the effects of exposure time on penetration rate for runs one through six taken from Table 7.

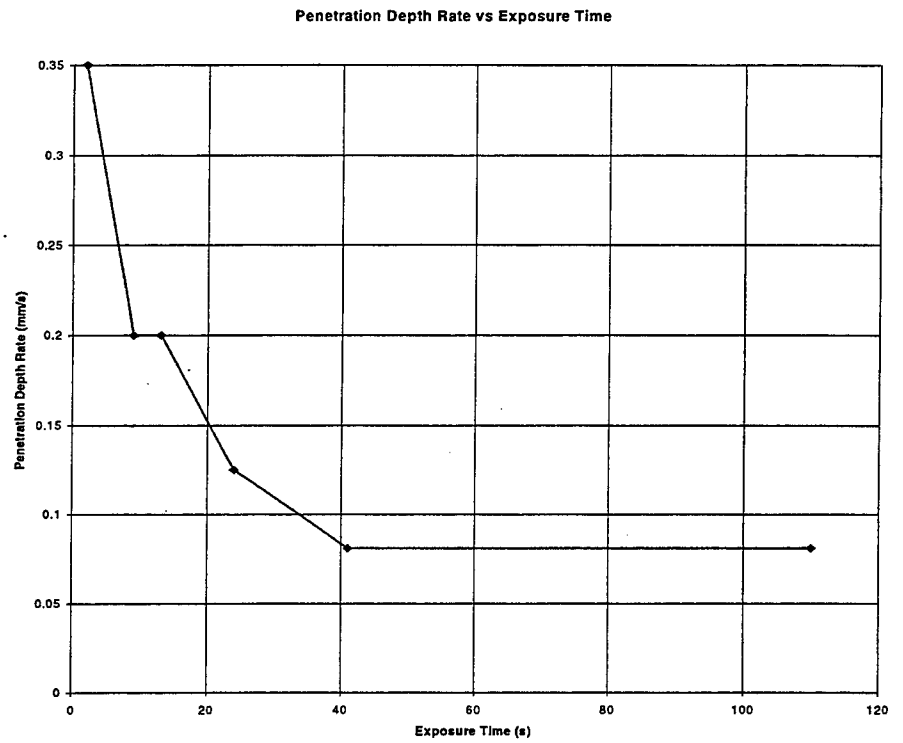

Figure 16. Exposure Time vs. Penetration Depth Rate for Fused Silica.

As the exposure time was increased more smoke and debris filled the hole and blocked the path of the laser beam causing the penetration rate to decline over time. Apparently 10kW/cm^2 is not a high enough intensity for this material to reach vaporization temperature. The heat was able to diffuse away quickly enough that the material reached a steady state in the liquid form, and would not clear for additional penetration. In the future, additional experiments can explore whether higher intensities, or altering the FEL wavelength during sample irradiation improves penetration rates through smoke and debris.

Since the second run was the only run at 9 kW/cm^2 to burn completely through the material at the primary power density of interest, it is worth a closer look. A digital picture of damage from run two was taken through an optical microscope as shown in Figure 17.

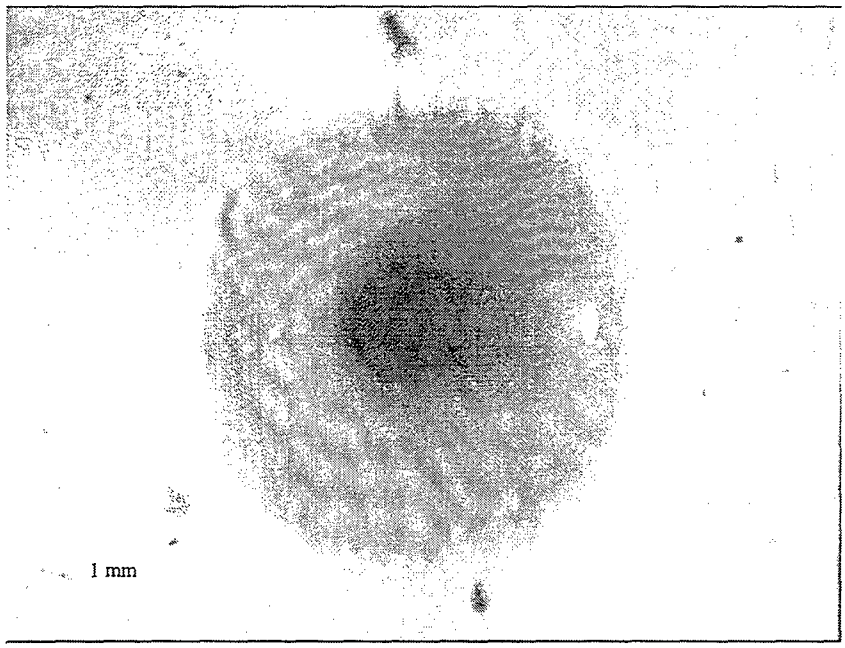

Figure 17. Close-Up of Damage to Slip-Cast Fused Silica Run 2.

Although the beam diameter was only 1.1 mm, the melted portion at the surface of the sample measured 5 mm in diameter. The hole is tapered with the melted portion on the back of the sample measuring only 2 mm in diameter. Since the sample face is 26 mm in front of the focus, and the sample back is 17mm from the focus, the beam size is decreasing as it proceeds through the material as shown in Figure 18. Also, the frontal area is irradiated longer than the back of the sample allowing for more time to expand the damage radially.

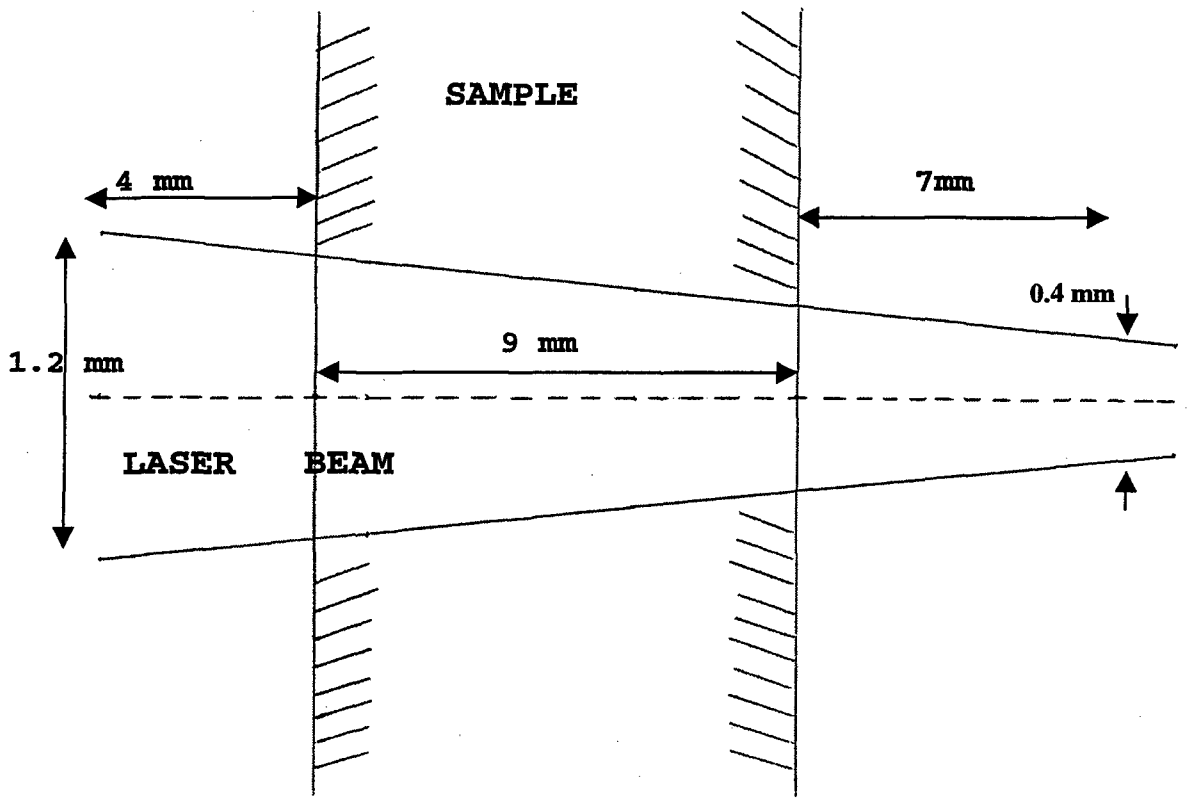

Figure 18. Sketch of Beam Focusing Effect.

The vertical scale in Figure 18 is exaggerated by a factor of five with respect to the horizontal scale in order to more clearly demonstrate the effect.

Examination of the hole from run two through an optical microscope reveals a 1-mm thick layer of melted and rehardened SiO_2 filling the hole at the back of the sample. It was clear from the video and the rear power meter that burn-through occurred in run two, but melted material solidified and resealed the hole at the back of the sample.

A picture of the back of the target taken through a Scanning Electron Microscope (SEM), Figure 19, shows the hole from run seven is fairly irregular with a great deal of debris.

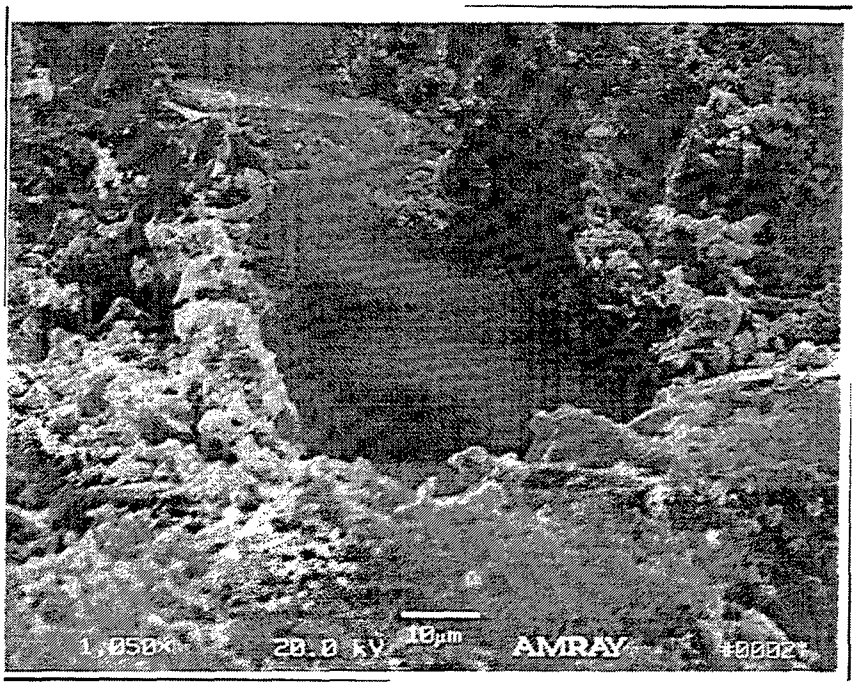

Figure 19. SEM Photograph of Damage to Fused Silica Run 7.

The volume of the hole in run two is estimated by,

$$V = \int_0^{9\,\mathrm{mm}} \pi[R(z)]^2 dz, \tag{14.}$$

where the radius approximately changes linearly as

$$R(z) = 0.53\ \mathrm{mm} - 0.02\ z[\mathrm{mm}], \tag{15.}$$

which gives a volume of $V = 5.6\ mm^3$. By a similar calculation, the volume of the entire damaged region, including the melted and rehardened portion, is estimated to be $V = 92\ mm^3$. Based on the density of fused silica of $\rho = 2.2\ g/cm^2$, the amount of material removed was 0.012 g, and the amount of material damaged was 0.20 g. The heat energy deposited during run two is given by,

$$E = P\tau = \Phi A\tau, \tag{16.}$$

which gives $E = 9.7$ kJ deposited during the 110 second run.

The predictions made in Chapter II, section A, indicated that this material could be burned through in about 3 seconds at 3 kW/cm^2, or just over 1 second at the 9 kW/cm^2 used in these experiments. Using these numbers in equation (16.) estimates that the energy that would need to be deposited to melt through this sample is only 95 Joules vice the 9.7 kJ that was actually deposited.

The amount of energy needed can also be calculated using the first method in Chapter II. That is by calculating the energy needed to break each bond of the SiO_2 molecules. The atomic weight of SiO_2 is 60 amu, or 1×10^{-22} g. Since the density of SiO_2 is $2.2\ g/cm^3$, the number of molecules per cubic centimeter is approximately 2×10^{22}. The required energy to break all the bonds assuming approximately 4 eV/bond is

$$E = \left(2.2 * 10^{22} \text{bonds} / \text{cm}^3\right)\left(4\text{eV} / \text{bond}\right)\left(1.6 * 10^{-19} \text{J} / \text{eV}\right) = 12.8 \text{ kJ} / \text{cm}^3 \quad (17.)$$

and using the volume calculated from equation (14.), the total energy required is predicted to be

$$E_T = \left(12.8 \text{ kJ} / \text{cm}^3\right)\left(5.6 \cdot 10^{-3} \text{cm}^3\right) \approx 72 \text{ J} \quad (18.)$$

which is very close to the 95 J predicted in above, but far from the 9.7 kJ delivered during the irradiation.

The difference in predicted and actual energy requirements seems to come about as a result of the change in state of the material. The calculations used in Chapter II and in the paragraphs above assume that the thermal diffusion length is small compared to the beam diameter. This is true for Slip-Cast Fused Silica in its normal state, where the thermal diffusion length was calculated in Chapter III, section B to be only 0.02 mm. However, it is possible that once the material melted, the thermal conductivity increased dramatically, increasing the thermal diffusion length substantially. This would result in a dramatic decrease in the amount of heat remaining in the area of the laser spot, and prevent the material from reaching the vaporization temperature. This seems to be what is taking place since even after being irradiated for 110 seconds, the

material still contains a large volume of melted and re-solidified material.

In future studies it would be interesting to note what intensity level is required in order for this material to reach vaporization temperature.

b) August 1999 Sample 1

The sample of slip-cast fused silica used in the August 1999 experiments measured 2.2 cm by 7.4 cm and had a variation in thickness from 0.9 to 1.9 cm. Figure 20 shows two sets of three irradiations done on the front face of the sample. The lower set of irradiations was done while air was blowing across the front surface of the sample, and the upper set without air. Table 8 shows the data and the results of these irradiations. Runs number 1,2 and 3 refer to the upper set of irradiations, and 4,5 and 6 to the lower set.

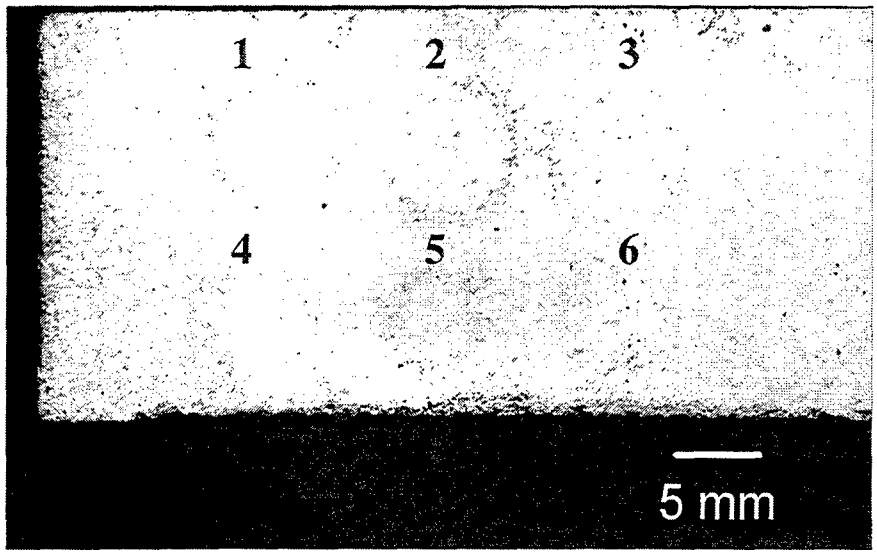

Figure 20. Slip-Cast Fused Silica Sample 1.

Table 8. Irradiation Data of Slip-Cast Fused Silica Sample 1.

Run Number	Wavelength (μm)	PRF (MHz)	Airflow (mph)	Average Power (Watts)	Average Intensity (W/cm^2)	Laser Beam Diameter (mm)	Damage Diameter (mm)
1	3.10	18.7125	No	105	490	5	6.2
2	3.10	18.7125	No	105	490	5	6.5
3	3.10	18.7125	No	105	490	5	6.0
4	3.10	18.7125	60	105	490	5	5.0
5	3.10	18.7125	60	105	490	5	5.0
6	3.10	18.7125	60	105	490	5	5.5

The exposure time of the above irradiations was 5 sec, and the energy per pulse was twice that of the measurements made in March 99. The damage diameters were measured using

an optical microscope. Due to the low average intensity ($490 W/cm^2$), we observed faint cyclic profiles on the sample material after the irradiations, whose diameters matched the calculated beam diameter reasonably well [Ref. 23]. The damage was just superficial, and the effect of the airflow was to decrease the diameter of the damage area, probably due to the rapid cooling of the sample by the air. Figure 21 shows a close up of damage in run 2.

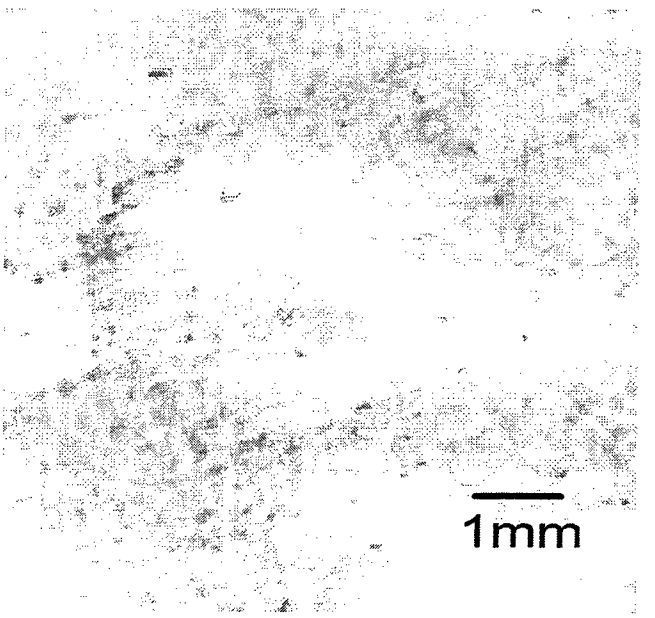

Figure 21. Close-Up Damage to Slip-Cast Fused Silica Run 2.

c) August 1999 Sample 2

The sample measured 2.2 cm by 7.4 cm and had a variation in thickness from 0.9 to 1.9 cm. Figure 22 shows the irradiations done on the front face of the sample and Table 9 the corresponding data.

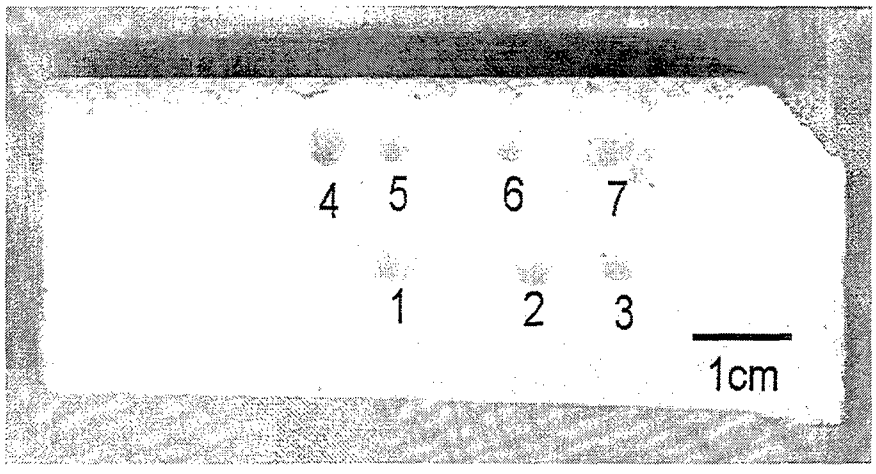

Figure 22. Slip-Cast Fused Silica Sample 2.

Table 9. Irradiation Data of Slip-Cast Fused Silica Sample 2.

Run Number	Wavelength (μm)	PRF (MHz)	Airflow (mph)	Average Intensity (kW/cm^2)	Laser Beam Diameter (mm)	Damage Diameter (mm)	Penetration Rate (mm/s)
1	3.10	18.7	No	10	1.76	3.8	0.29
2	3.10	18.7	No	10	1.76	3.5	0.30
3	3.10	18.7	No	10	1.76	3.5	0.32
4	3.10	18.7	60	10	1.76	3	0.34
5	3.10	18.7	60	10	1.76	3	0.33
6	3.10	18.7	60	10	1.76	2.5	0.31
7	3.10	18.7	No	10	1.76	3.9	0.29

The average beam power was 105 Watts. The exposure time for the above irradiations was 5 sec, and the average intensity was 10 kW/cm^2. The average damage diameter, for the irradiations done in the presence of airflow, was 2.83

mm and for those without airflow was 3.67 mm. Again the damage diameters matched the calculated beam diameters reasonably well, and the effect of the presence of air was to decrease the diameter of the damaged area [Ref. 23]. No burn-through occurred during the irradiations. The damage produced on the sample had the shape of small cyclic crater. The areas around the craters were clean of debris. Part of the melted material was evaporated during the irradiation and the rest of it remained inside the crater.

The average penetration rate, for the irradiations done in the presence of airflow, was 0.326 mm/s and for those without airflow was 0.3 mm/s. The presence of airflow only slightly increased the penetration rate.

The data from Figure 16 is shown again in Figure 23, and shows the effects of the exposure time on penetration depth rate.

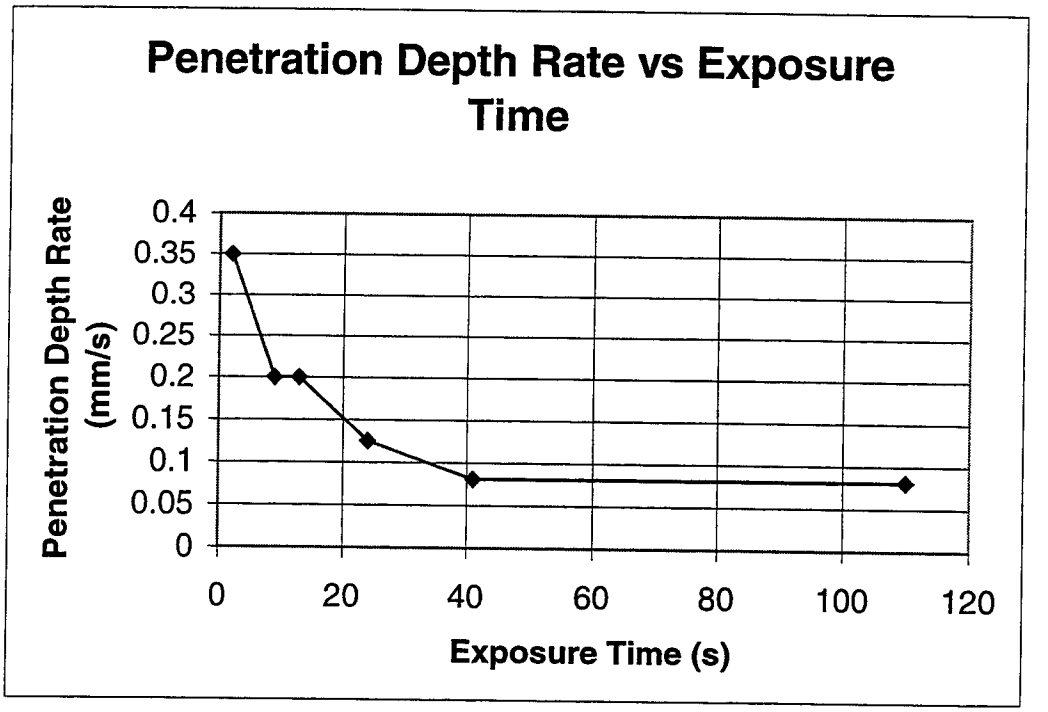

Figure 23. Exposure Time vs. Penetration Rate for Fused Silica March 1999.

The average power of the March 1999 experiment was 100 to 103W±5W, the wavelength λ=4.825 µm, average intensity 10 kW/cm^2, and PRF 37.4 MHz. As can be seen from Figure 23, the penetration depth rate that corresponds to an exposure time of 5 sec is approximately 0.26 mm/s. Table 9 shows that when the PRF is 18.7 MHz and the wavelength is λ=3.10 µm, the penetration rate is just slightly faster than either with the presence of airflow or without it. It is true that when the PRF is lower there is higher fluence per pulse and thus intensity per micropulse, but this increase in burn rate is too small to draw any definite conclusions concerning PRF or pulse length effects.

In the future it would be interesting to conduct experiments changing just one parameter in each experiment, and irradiate all the samples for the same length of time, so that we can better evaluate the effect the change of individual parameters have on the burn through rates.

d) March 2000

The purpose of the March 2000 experiments was to increase the size of the laser beam spot while maintaining the same intensity of 10 kW/cm^2. To do this the average beam power was increased to 500 Watts. The sample of slip-cast fused silica was the same used in the March 1999 experiments. It measured 6.9 cm by 7.4 cm and had a variation in thickness from 0.9 to 1.9 cm. Figure 24 shows the irradiations done on the front face of the sample and Table 10 the corresponding data. The two new irradiations conducted in this experiment are labeled 1 and 2 in Figure 24.

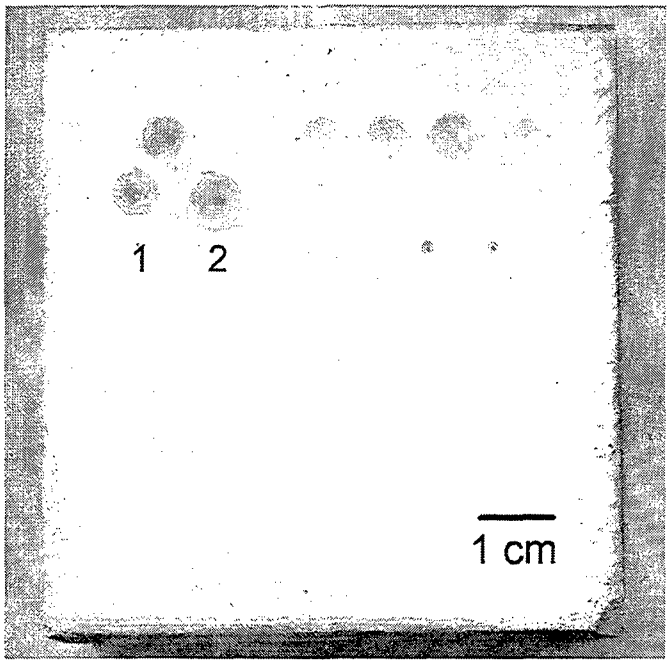

Figure 24. Slip-Cast Fused Silica Sample 3.

Table 10. Irradiation Data of Slip-Cast Fused Silica Sample 3.

Run Number	Wavelength (μm)	PRF (MHz)	Airflow (mph)	Average Intensity (kW/cm^2)	Laser Beam Diameter (mm)	Damage Diameter (mm)	Penetration Rate (mm/s)
1	3.10	37.425	83-86	10	2.4	4.4	1.32
2	3.10	37.425	No	10	2.4	5.6	7.5

Burn-through of the material occurred during the above irradiations. The burn-through time for Run 1 was 6.8 sec and for Run 2 was 1.2 sec. In Run 1, the damage diameter on the front face of the material sample was 4.4 mm, and on the back face was 3.1 mm. In Run 2 the damage diameter on the

front face was 5.6 mm and on the back face 1.8 mm. It can be seen that the effect of airflow was to reduce the front face damage diameter and to increase the burn-through time. Apparently the airflow is not removing material, but only cooling the sample.

It can also be seen that the back face damage diameters of the material sample are smaller than the front face. There are three possible explanations for this. The first is that the beam profile follows the Gaussian distribution, with the highest intensity in the center of the beam and intensity down by 1/e at the beam radius. The second is the position of the sample. The sample is 9 mm thick and was located during the irradiations 217.0 mm from the back surface of the lens while the back focal length of the lens was 235.7 mm. It was 18.7 mm from the focus, so the beam size is decreasing as it proceeds through the material. The third is that the front surface is exposed to irradiation for longer time than the back.

The volume of the entire damaged region in Run 1 is estimated by,

$$V_{IT} = \int_0^{9mm} \pi \cdot R_{IT}^2(z) \cdot dz \,, \qquad (19.)$$

where the radius changes approximately linearly as

$$R_{1T}(z) = 2.2\text{mm} - 0.072 \cdot z[\text{mm}] \qquad (20.)$$

The volume of the entire damaged region in Run 2 is estimated by,

$$V_{2T} = \int_0^{9\text{mm}} \pi \cdot R_{2T}^2(z) \cdot dz \qquad (21.)$$

where the radius changes approximately linearly as

$$R_{2T}(z) = 2.8\text{mm} - 0.211 \cdot z[\text{mm}] \qquad (22.)$$

After doing the above calculations the volume of the entire damage region in Run 1 is V_{1T}=100.5 mm^3 and in Run 2 is V_{2T}=105.3 mm^3. Knowing that the density of the fused silica is ρ=2.2 g/cm^3 the mass of the entire damaged region in Run 1 is m_{1T}= 0.221 grams and in Run 2 is m_{2T}=0.232 grams. The volume of the hole in Run 1 is estimated by,

$$V_{1H} = \int_0^{9\text{mm}} \pi \cdot R_{1H}^2(z) \cdot dz, \qquad 23.)$$

where the radius changes approximately linearly as

$$R_{1H}(z) = 1.6\text{mm} - 0.1167 \cdot z[\text{mm}] \qquad (24.)$$

The volume of the hole in Run 2 is estimated by,

$$V_{2H} = \int_0^{9mm} \pi \cdot R_{2H}^2(z) \cdot dz \qquad (25.)$$

where the radius changes approximately linearly as

$$R_{2H}(z) = 0.75mm - 0.0444 \cdot z[mm] \qquad (26.)$$

After doing the above calculations the volume of the hole in Run 1 is V_{1H}=35.2 mm^3 and in Run 2 is V_{2H}=8.9 mm^3. Knowing that the density of the fused silica is ρ=2.2 g/cm^3 the mass of the material removed creating a hole in Run 1 is m_{1H}=0.078 grams and in Run 2 is m_{2H}=0.020 grams.

These calculations show that the damaged regions, either with or without the presence of airflow, have approximately the same volume ($V_{1T=}$100.5 mm^3 and $V_{2T=}$105.3 mm^3). The basic effect of the airflow is that it increases the volume of the hole of the damaged region (V_{1H}=35.2 mm^3 and V_{2H}=8.9 mm^3).

Table 11 shows the burn-through irradiation data of an older experiment conducted on the same sample of fused silica without the presence of air and analyzed in Ref 23.

Table 11. Irradiation Data of March 1999 Slip Cast Fused Silica Sample 3.

Run Number	Wavelength (μm)	PRF (MHz)	Average Power (Watts)	Average Intensity (kW/cm^2)	Volume of entire damaged region (mm^3)	Volume of the hole (mm^3)	Penetration Rate (mm/s)
2	4.825	37.425	100	10	92	5.6	0.081

Comparing the results of the March 2000 experiments with those on Table 11, we see that shifting the wavelength from λ=4.825 μm to λ=3.1 μm, and increasing the average power from 100 Watts to 500 Watts, the penetration rate increases dramatically from 0.081 mm/s to 1.32 mm/s with the presence of airflow and to 7.5 mm/s without it. The volume of the entire damaged region increases slightly from 92 mm^3 to 100.5 mm^3 with the presence of airflow and to 105.3 mm^3 without it. Finally the volume of the hole increases from 5.6 mm^3 to 35.2 mm^3 with the presence of airflow and to 8.9 without it.

A possible explanation for the success of the March 2000 runs is the increase in beam radius from 0.087cm to 0.12cm. This increase in beam area could be enough so that even with the large thermal diffusion length estimated in Section B.3.a. of this chapter, the new beam area was large enough to ensure enough heat was retained to reach vaporization.

Figure 25 shows a close-up of damage in run 1 and Figure 26 in run 2. Figure 27 shows the view of those irradiations on the back face of the sample.

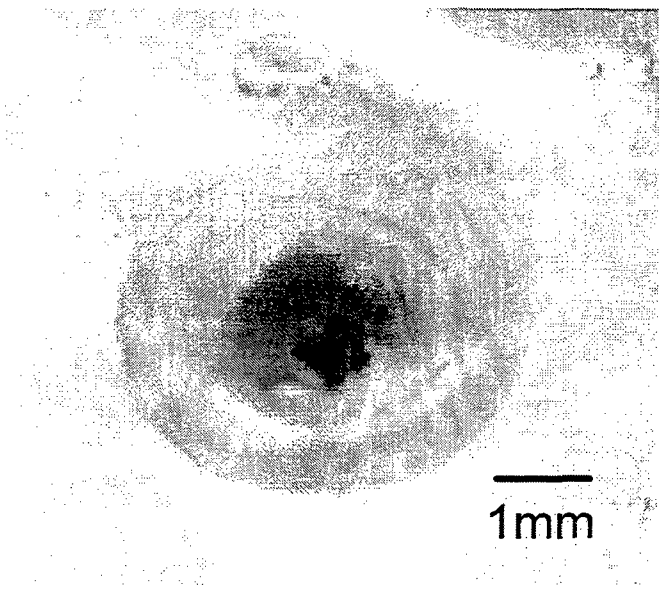

Figure 25. Close-Up of Damage of Slip Cast Fused Silica Run 1.

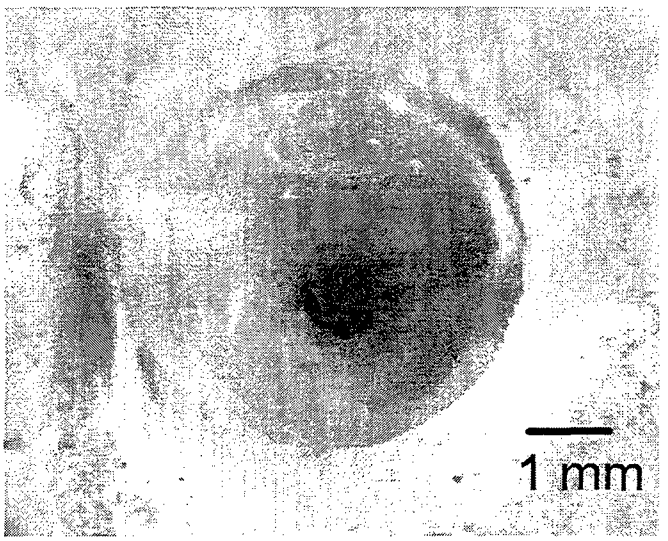

Figure 26. Close-Up of Damage of Slip-Cast Fused Silica Run 2.

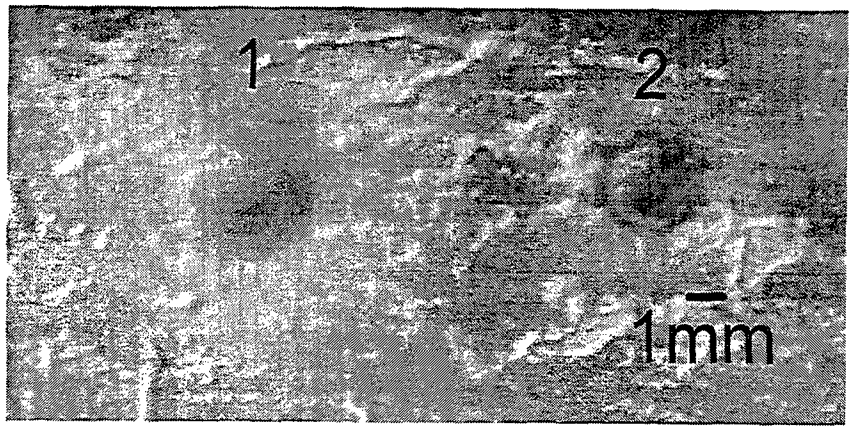

Figure 27. Back View of Damage to Slip Cast Fused Silica Runs 1 and 2.

4. Polyimide Fiberglass

a) March 1999

The sample provided by NRL was 11.4 cm by 10.1 cm and 2 mm thick. The damaged area of the sample, after irradiation, is shown in Figure 28.

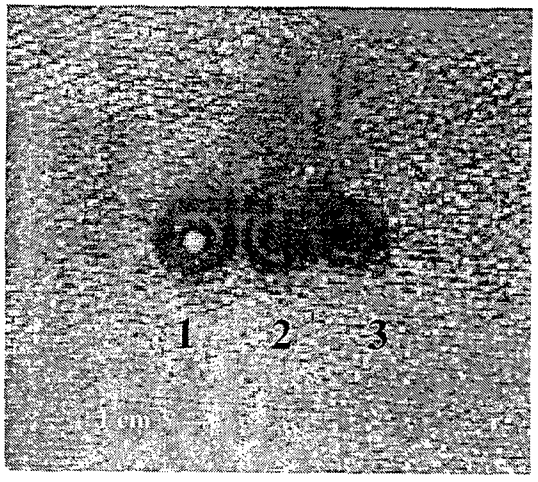

Figure 28. Polyimide Fiberglass.

The sample was irradiated three times and the results are summarized in Table 12.

Table 12. Irradiation of Polyimide Fiberglass.

Run Number	Average Intensity (kW/cm^2)	Exposure Time (s)	Penetration Depth Rate (mm/s)
1	9	7	0.28
2	9	2	0.90
3	9	1	1.1

The irradiations were done from left to right with the sample 26 mm in front of the focus of the beam. Only the first run achieved burn-through of the material, with the entry hole 3 mm in diameter and the exit hole 1.5 mm. All three holes show significant charring which impedes damage. Investigation with an optical microscope reveals a raised lip of material around the face of the hole that does not appear on the fused silica sample. There is much more roughness as observed in Figure 29 to Figure 31. The charred region extends to a diameter of 8 mm for run one, 6.5 mm for run two, and 5.4 mm for run three. The lip height is 0.3 mm for run one, 0.1 mm for run two, and 0.05 mm for run three. These measurements indicate that as the dwell time increases, the radial extent of the damage area increases, and more material is deposited around the edge of the hole. There is no evidence of melted and rehardened

material present in the holes as found with the fused silica indicating a different mechanism for damage in the two samples.

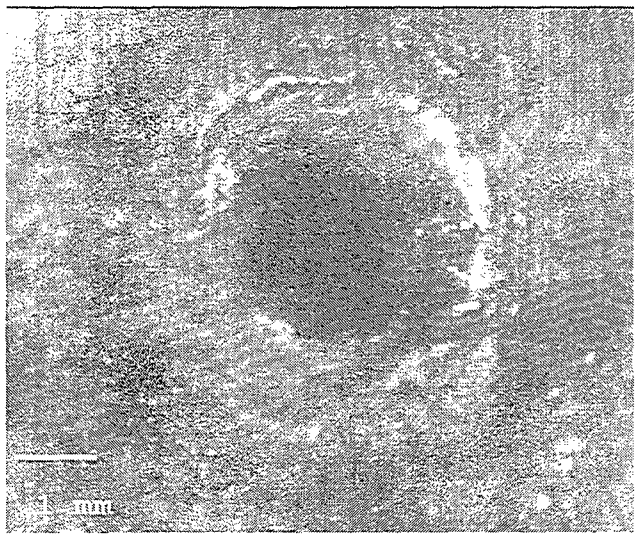

Figure 29. Close-Up of Damage to Polyimide Fiberglass Run 1.

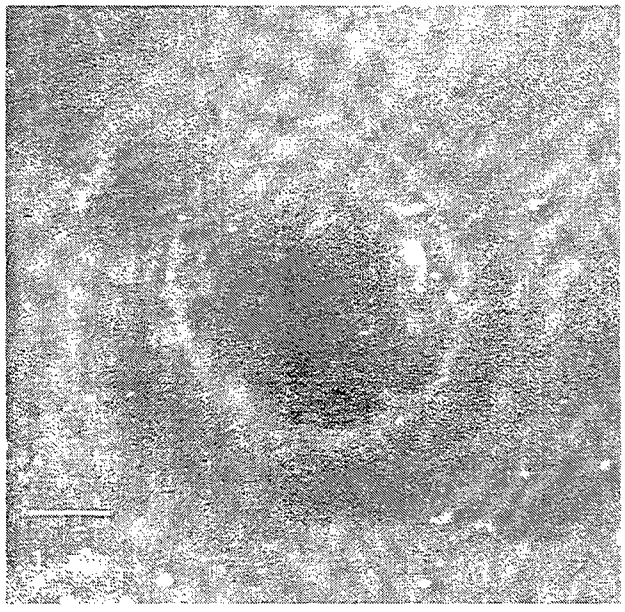

Figure 30. Close-Up of Damage to Polyimide Fiberglass Run 2.

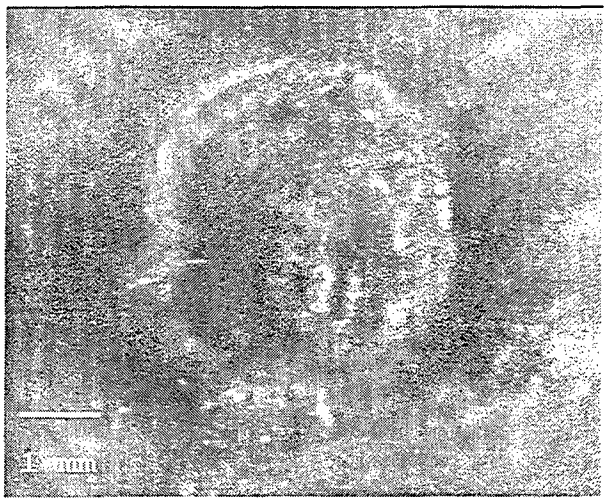

Figure 31. Close-up of Damage to Polyimide Fiberglass Run 3.

b) August 1999 and March 2000

The sample used in the March 1999 experiments was again used. It had dimensions 11.4 cm by 10.1 cm and 2 mm thickness. Figure 32 shows a photo of the sample after all sets of irradiations. Irradiations with numbers 1,2 and 3 were those conducted in March 1999, however the numbering order was accidentally reversed from that of Figure 28. Irradiations 4 to 15 were conducted in August 1999 and 16 to 21 were conducted in March 2000. All irradiations were done three times with the same parameters in order to get more accurate measurements. The actual results came from the mean value of the three measurements. Irradiations 7,8,9,10,11,12,16,17,18 were done with no airflow while in 4,5,6,13,14,15,19,20,21 there was airflow present.

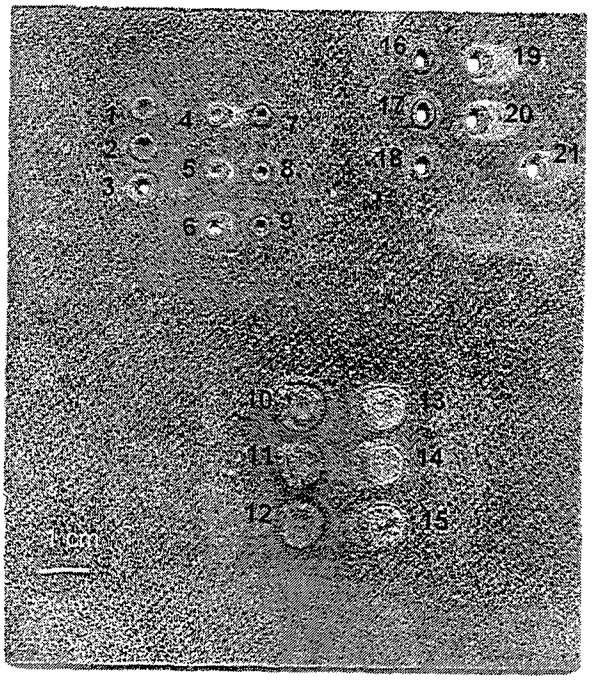

Figure 32. Polyimide Fiberglass (Front View).

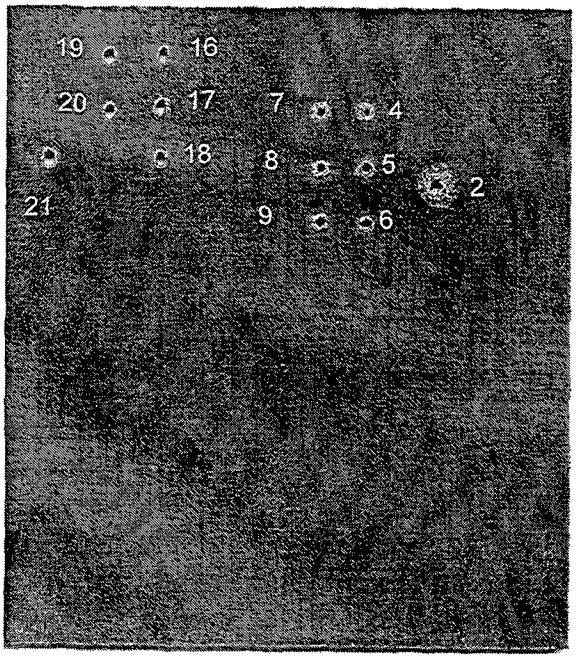

Figure 33. Polyimide Fiberglass (Back View).

In Figure 33 we see a photo of the backside of the sample showing that all of the 10 kW/cm^2 irradiations completely penetrated the sample. (Note: Hole 3 in Figure 32 has mistakenly been numbered 2 in Figure 33). On the other hand the 500 W/cm^2 intensity (irradiations 10 to 15 of Figure 32 did not penetrate the sample. Irradiation results are summarized in Table 13. Each row represents a set of three irradiations.

Table 13. Polyimide Fiberglass Irradiation Results.

Hole Number	Average Power (W)	Average Intensity (kW/cm^2)	PRF (MHz)	λ (μm)	Spot radius (mm)	Airflow (mph)	Burn through time (sec)	Penetration Depth Rate (mm/sec)	Front Damage Pattern	Entry Hole Diameter (mm)	Rear Damage Pattern	Exit Hole Diameter (mm)
10,11,12	100	0.5	18.7	3.1	2.5	No	4.5 *	0.3	Circular	4.4	---	---
13,14,15	100	0.5	18.7	3.1	2.5	60	4.5 *	0.3	Circular	6.6	---	---
7,8,9	100	10	18.7	3.1	0.87	No	1.4	1.4	Circular	1.7	Circular	1.3
4,5,6	100	10	18.7	3.1	0.87	60	1.2	1.6	Circular	1.9	Circular	1.4
16,17,18	500	10	37.4	3.1	1.25	No	0.40	5.0	Elliptical	3.5 x 2.5	Elliptical	2.5 x 1.5
19,20,21	500	10	37.4	3.1	1.25	85	0.35	5.7	Elliptical	3.7 x 2.9	Elliptical	2.6 x 1.7

* There was no burn through. The time indicated is the exposure time.

The hole diameters and the penetration depth rates have variations of 0.3 mm and 0.5 mm/sec respectively from the mean value subtended by the measurements made in each set of three holes. This is due to the slight variation of the exposure time, which is on the order of 1 to 2 seconds.

The following table presents the results of the experiment conducted in March 1999 (Holes 1,2,3).

Table 14. Irradiation of Polyimide Fiberglass, March 1999

Average Power (W)	Average Intensity (kW/cm^2)	PRF (MHz)	λ (μm)	Spot radius (mm)	Airflow (mph)	Penetration Depth Rate (mm/sec)
1	9	37.4	4.825	0.87	NO	0.28
2	9	37.4	4.825	0.87	NO	0.90
3	10	37.4	4.825	0.87	NO	1.1

The above results have the same irradiation parameters with those of runs 7,8, and 9 of Table 13 except for the PRF and the wavelength. Comparing run 1 of Table 14 (the only one to be irradiated until burn through) with runs 7, 8, and 9 of Table 13, it appears that the shorter (λ=3.1 μm) wavelength combined with the lower PRF is much more effective, resulting in 500% higher penetration depth rate. The lower PRF apparently causes more damage, since it results in more energy per pulse for the same pulse length.

The presence of airflow resulted in 15% bigger hole diameter and penetration depth rate than those attained without air. The larger spot size irradiations conducted with 500 W average power (runs 16 to 21), caused 3.5 times higher penetration depth rate than the ones conducted with 100 W (runs 4 to 9), even though both were at the same intensity level. This could be because the larger spot allows material to exit the region quicker, or because the larger spot better meets the thermal diffusion requirement discussed in Chapter III.

The damage pattern of runs 16 to 21 is not circular as expected but somewhat elliptical, which is very clear in Figure 38 to Figure 41, which present a closer view of the damage caused by the irradiations.

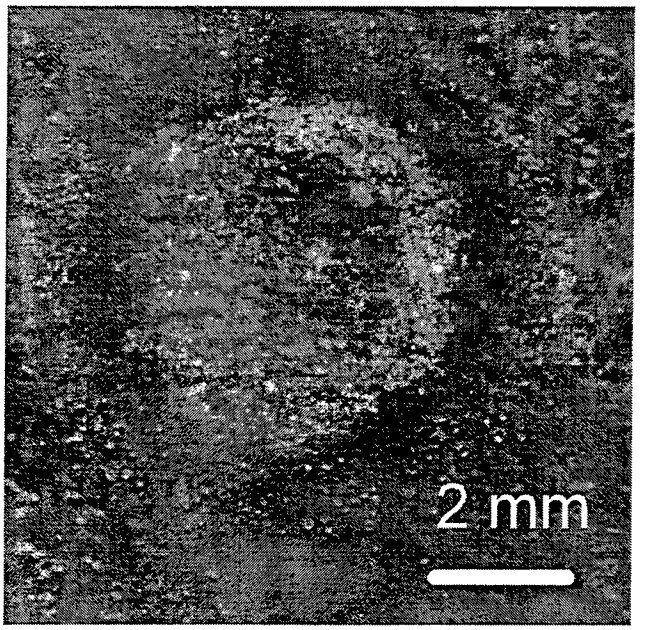

Figure 34. Polyimide Fiberglass Run 12.

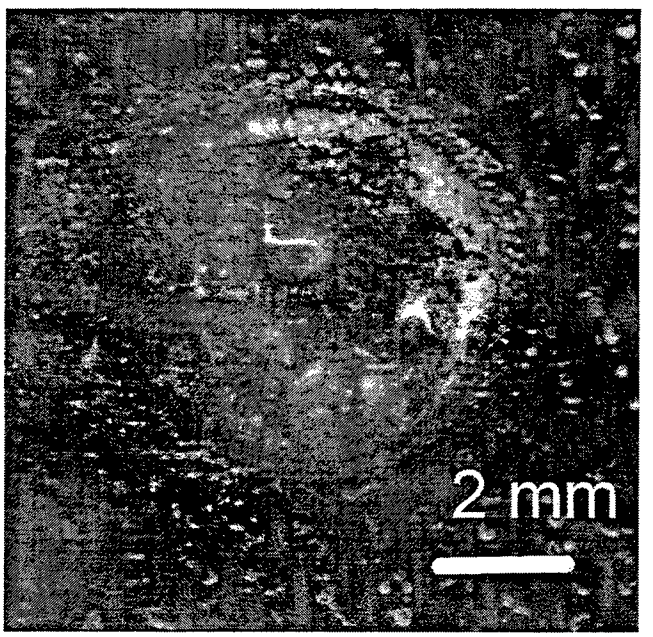

Figure 35. Polyimide Fiberglass Run 15.

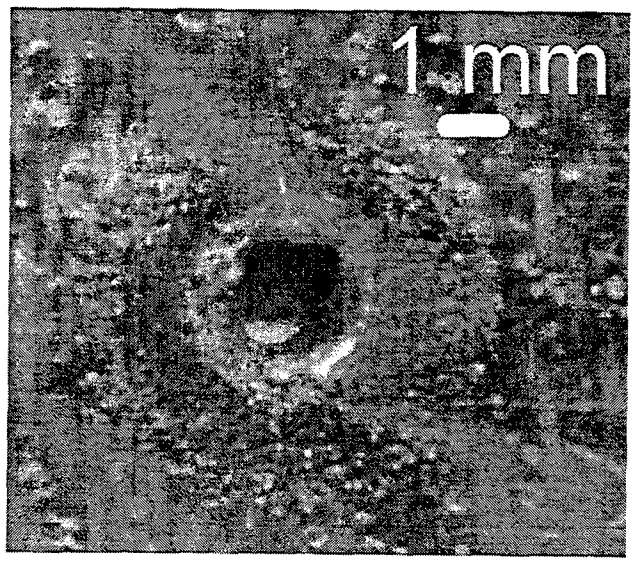

Figure 36. Polyimide Fiberglass Run 8.

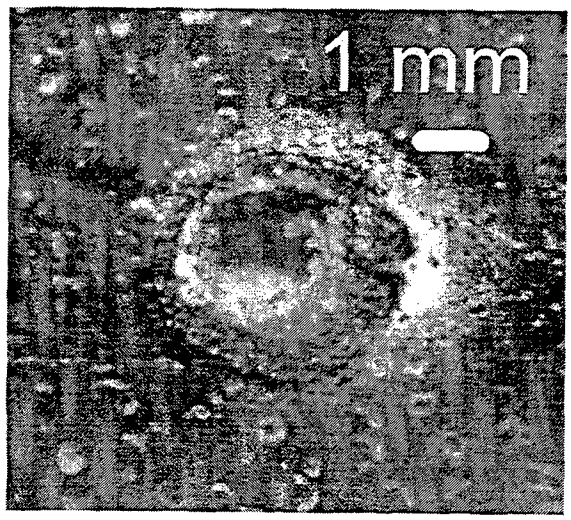

Figure 37. Polyimide Fiberglass Run 5.

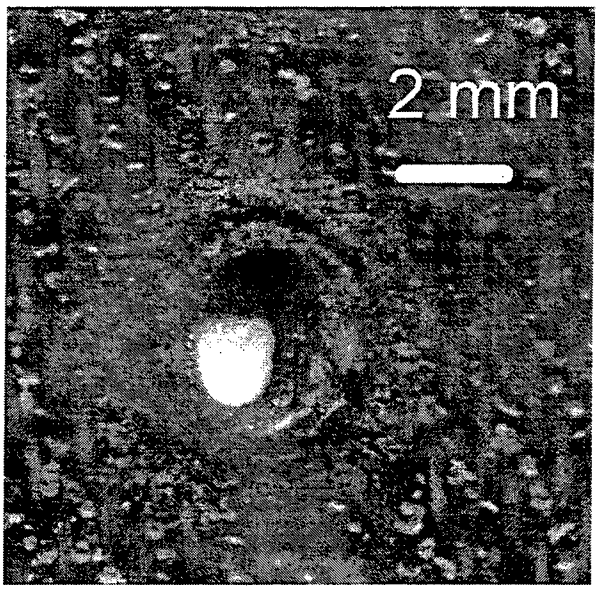

Figure 38. Polyimide Fiberglass Run 18.

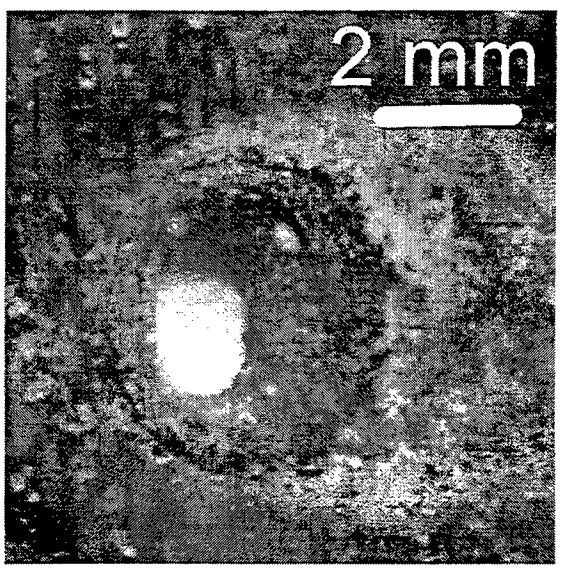

Figure 39. Polyimide Fiberglass Run 20.

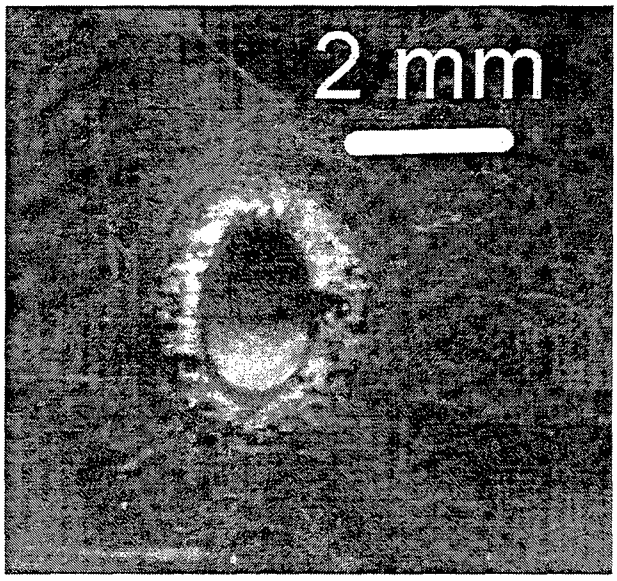

Figure 40. Polyimide Fiberglass Exit Hole Run 18.

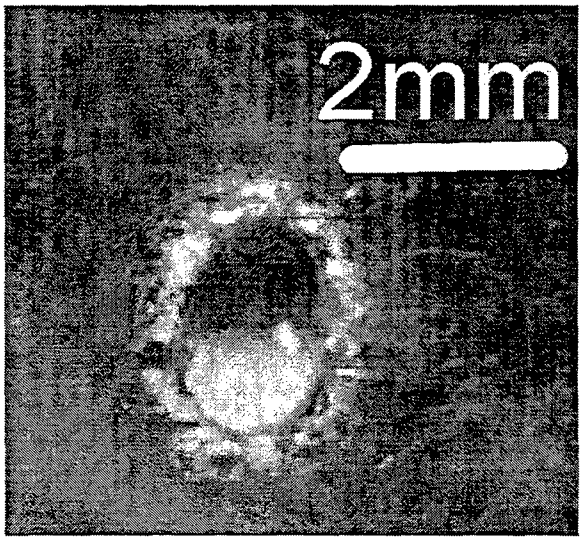

Figure 41. Polyimide Fiberglass Exit Hole Run 20.

In all cases a raised lip of melted material is observed around the face of the entrance hole. The dimensions of the lip are approximately 0.2 mm in height and 1mm in width. However, when airflow is present the lip tends to be smaller, possibly because the airflow removes the debris and the evaporated material that actually contributes to the formation of the lip. This would explain the bigger diameter of the holes made in the presence of airflow, since the diameter is measured from the inside part of the lip.

The charred region extends approximately 2mm around the lip when there is no airflow. With airflow this area is much smaller. The charred region around the exit hole extends to 1 to 1.5 mm in all cases, as the backside of the sample was not exposed to the airflow. As the exposure time is increased the radial extent of the damaged area is increased and more melted material was deposited around the hole. After the irradiation stopped there was a period of almost 3 sec that the material is still hot and melting. The airflow tends to increase the rate of cooling of the material, decreasing the material was hot and melted almost in half, and resulting in less melted material.

Investigation with a microscope reveals that there is no evidence of melted or rehardened material inside the holes. It is also evident that the damage is most significant in the center of the hole, diminishing radially

outward, which supports expectation of a Gaussian shape of the laser beam intensity.

5. F2 Epoxy

a) March 1999

The sample of F2 Epoxy provided by NRL was 10.0 cm x 11.5 cm and 1.5-mm thick including a 1.6-cm thick polyurethane foam backing. The damaged area of the sample, after irradiation, is shown in Figure 42.

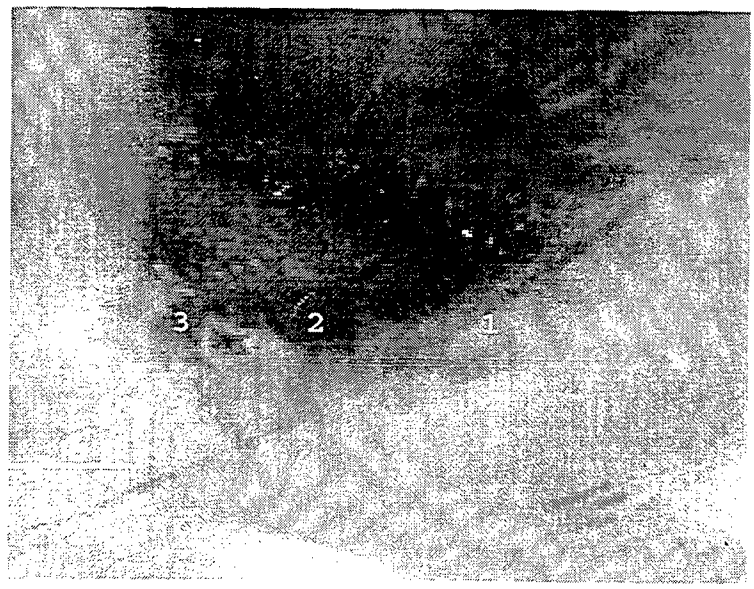

Figure 42. F2 Epoxy Sample.

The sample was irradiated three times and the results are summarized in Table 15.

Table 15. Irradiation of F2 Epoxy.

Run Number	Average Intensity (kW/cm^2)	Time (s)	Penetration Depth Rate (mm/s)
1	9	11	0.10
2	9	6	0.12
3	9	3	0.10

In each case, it appears that the F2 Epoxy was completely penetrated, and the damage of the foam backing had begun, but had not been completed. The videotape showed flames engulfing the upper portion of the sample and Figure 42 shows the black charred area extending to the edge of the sample. Significant charring was evident when the sample was viewed with the optical microscope. This charring was very similar to the Polyimide sample. There was also evidence of some melting, but not as much as occurred in the Fused Silica sample. The holes appear to be filled with the charred debris of the polyurethane backing, making hole depth measurements difficult and rendering penetration depth rates unreliable. Figure 43 to Figure 45 show the details of runs one through three.

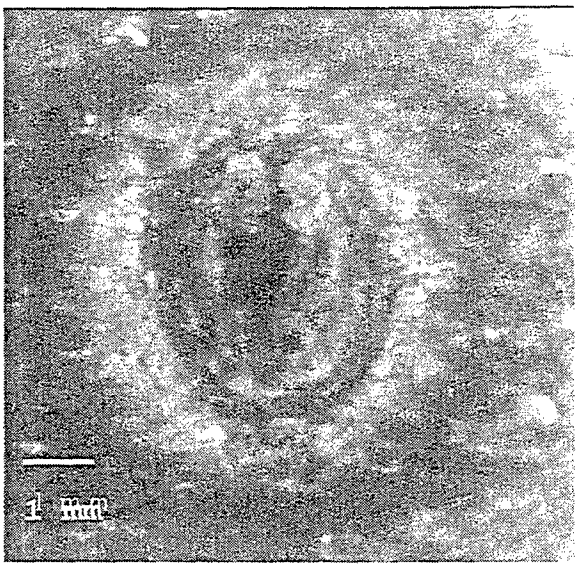

Figure 43. Close-Up of Damage of F2 Epoxy Run 1.

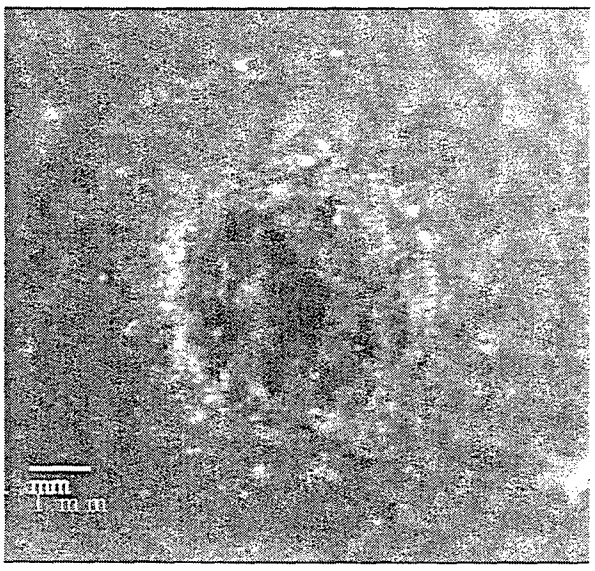

Figure 44. Close-Up of Damage of F2 Epoxy Run 2.

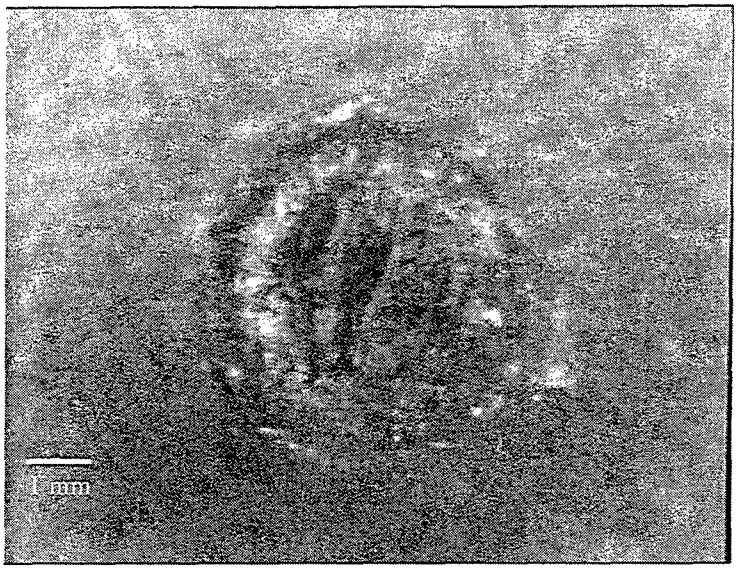

Figure 45. Close-Up of Damage to F2 Epoxy Run 3.

The damaged region extends to a diameter of 11.3 mm for run one, 7.5 mm for run two, and 5.2 mm for run three. There is a lip around each of the holes, but much smaller than the Polyimide sample. The lip for run one was 0.05 mm in height. For runs two and three, the lip was too small to measure with the optical microscope mechanism. These measurements indicate that as dwell time increases the radial extent of the damage area increases, and more material is deposited around the edge of the hole. When airflow is added to the test, debris may be removed from the hole during irradiation.

b) August 1999 and September 2000

The sample had dimensions 11.5 cm by 10 cm and 1.5 mm thickness, attached to a 1.6-cm thick polyurethane foam

backing (Figure 47). In Figure 46, we see the front of the sample after all sets of irradiations. Irradiations with numbers 1, 2 and 3 were those conducted in March 1999. Irradiations 4 to 15 were conducted in August 1999 and 16 to 21 were the last ones conducted in March 2000. Following the same procedure as with Polyimide, all the irradiations were done three times with the same parameters in order to get more accurate measurements. The results presented here came from the mean value of the three measurements. Irradiations 7 through 12, 16, and 17 were done with no airflow while in 4,5,6,13,14,15,19,20 and 21 there was airflow present. In Figure 48, we see the backside of the sample showing that all of the 10 kW/cm^2 irradiations completely penetrated the sample. On the other hand the 500 W/cm^2 intensity (runs 4 to 9) did not penetrate. However, they caused more extensive surface damage due to the bigger spot radius.

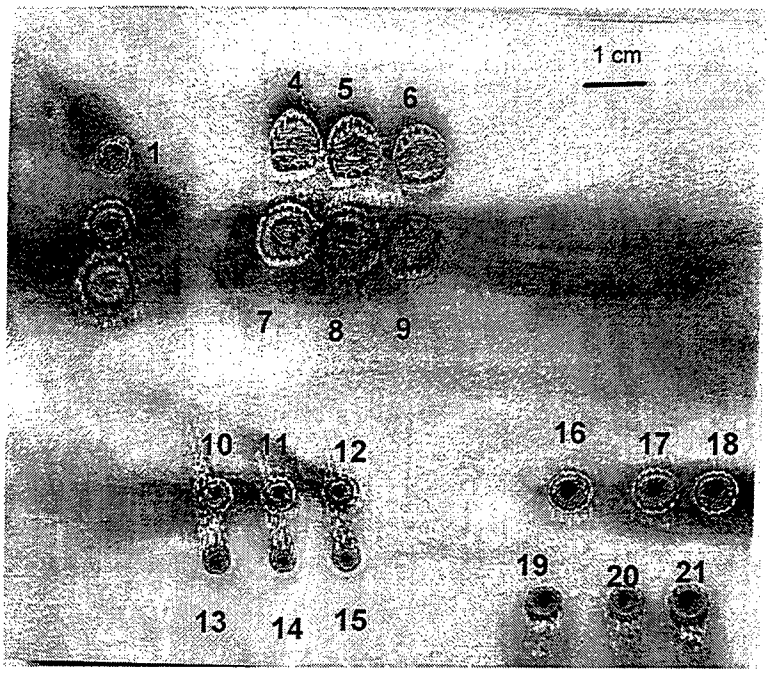

Figure 46. F2 Epoxy (Front View).

Figure 47. F2 Epoxy (Side View).

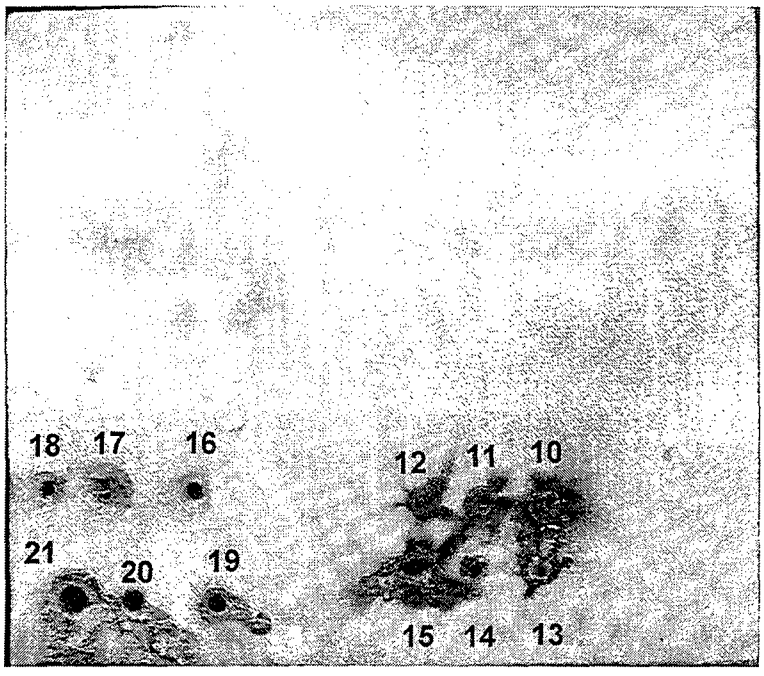

Figure 48. F2 Epoxy (Back View).

The presence of the foam layer at the backside of the sample made the measurements of the exit holes diameter unreliable. A closer caption of the damage is presented in Figure 49 through Figure 54.

Irradiation results are summarized in Table 16. Each row of the table represents a set of three irradiations, conducted with the same characteristics.

Table 16. F2 Epoxy Irradiations Results.

Hole Number	Average Power (W)	Average Intensity (kW/cm^2)	PRF (MHz)	λ (μm)	Spot radius (mm)	Airflow (mph)	Burn through time (sec)	Penetration Depth Rate (mm/sec)	Front Damage Pattern	Entry Hole Diameter (mm)	Rear Damage Pattern	Exit Hole Diameter (mm)
7,8,9	100	0.5	18.7	3.1	2.5	No	3.5 *	0.1	Circular	8.7	---	---
4,5,6	100	0.5	18.7	3.1	2.5	60	4 *	0.1	Circular	7.2	---	---
10,11,12	100	10	18.7	3.1	0.87	No	2.5	0.6	Circular	4.0	Circular	1.2
13,14,15	100	10	18.7	3.1	0.87	60	2.5	0.6	Circular	2.6	Circular	1.1
16,17,18	500	10	37.4	3.1	1.25	No	1.1	1.4	Slightly elliptical	5.6 x 5.3	circular	2.0
19,20,21	500	10	37.4	3.1	1.25	85	1.0	1.5	Slightly elliptical	5.2 x 4.7	Slightly elliptica	2.2 x 1.8

* There was no burn through. The indicated time is the exposure time.

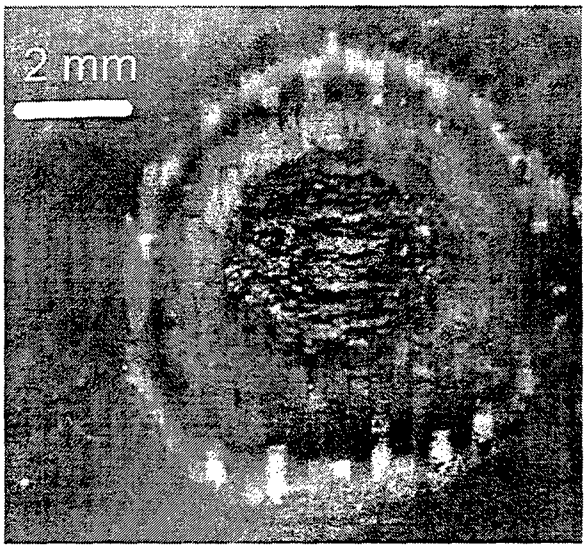

Figure 49. Close-Up of Damage to F2 Epoxy Run 7.

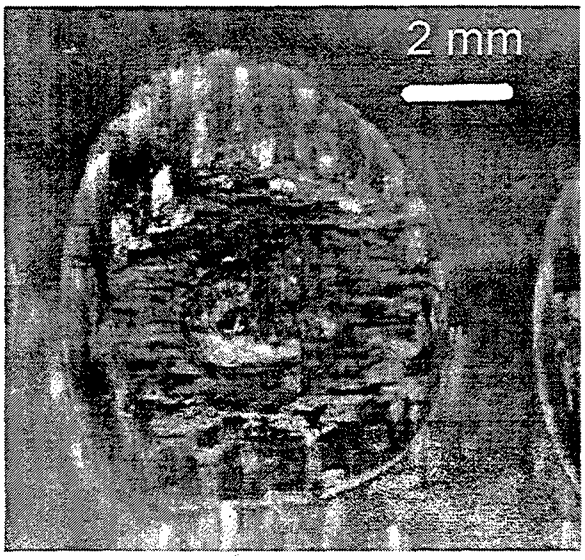

Figure 50. Close-Up of Damage to F2 Epoxy Run 5.

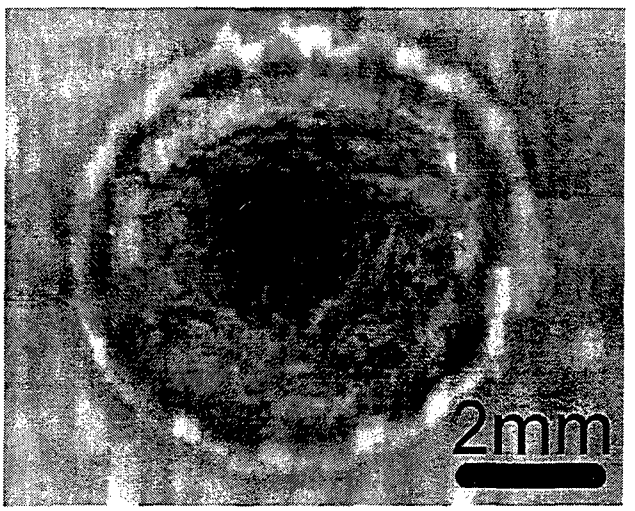

Figure 51. Close-Up of Damage to F2 Epoxy Run 16.

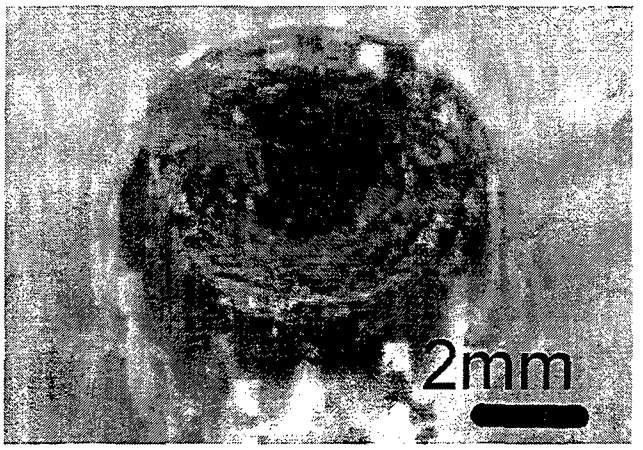

Figure 52. Close-Up of Damage to F2 Epoxy Run 20.

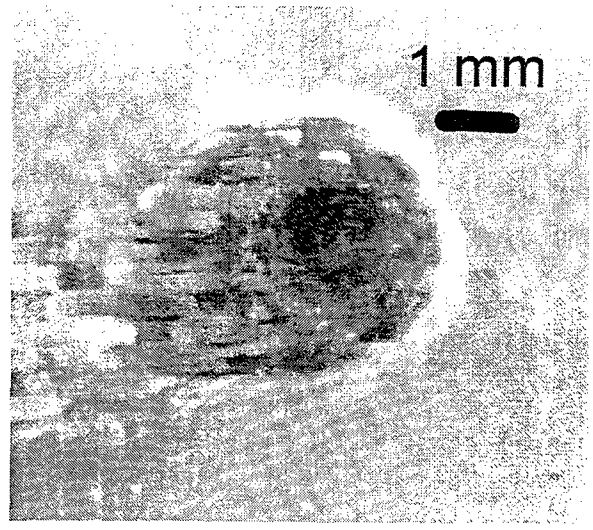

Figure 53. Close-Up to Damage of F2 Epoxy Run 12.

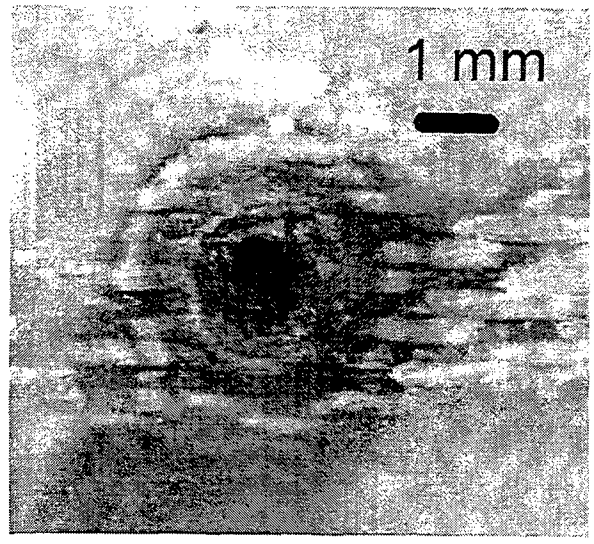

Figure 54. Close-Up Damage to F2 Epoxy Run 15.

The hole diameters have a variation of 0.5 mm from the mean value. This is again due to the slight variance of the exposure time of the irradiations, which is on the order of 1 to 2 seconds. With the presence of the entry hole diameter decreased by 10% to 30%.

Table 17. Irradiation Results of March 1999 Experiment on F2 Epoxy.

Run Number	Average Intensity (kW/cm^2)	PRF (MHz)	λ (μm)	Spot radius (mm)	Airflow (mph)	Penetration Depth Rate (mm/sec)
1	9	37.4	4.825	0.87	No	0.10
2	9	37.4	4.825	0.87	No	0.12
3	9	37.4	4.825	0.87	No	0.10

Table 17 shows the results of the March 1999 experiment. Comparing these results with runs 10 to 12 of Table 16, it is clear again that the λ=3.1 μm wavelength combined with the lower PRF was more effective, and resulted in six times higher penetration depth rate.

The average power of 500 W (runs 16 to 21), resulted in a higher penetration rate than the 100 W power (runs 10 to 15), and caused a slightly elliptical damage pattern.

Comparing runs 10,11,and 12 with runs 16,17, and 18 from Table 16, the penetration rate for the larger spot size was 230% greater than that of the small spot.

During the irradiation, flames, smoke, and debris covered the entrance hole. After the irradiation stopped the material was still burning for almost 3 seconds, which caused extra charring and melting of the sample. When airflow was applied, the time decreased by half. The charred region extends approximately 0.5 mm around the entrance hole with airflow present and 1 mm without airflow. Examination of the holes with a microscope revealed more roughness than with the Polyimide. This was probably caused by deposited debris and charred material. The Gaussian beam caused the same damage pattern with the Polyimide sample, being more intensive at the center of the spot. However the penetration rates were 2 to 3 times smaller.

VI. CONCLUSIONS

This report describes the first measurements of laser damage on missile materials from the newly developed TJNAF free electron laser. The report consolidates results from material damage studies and contains the work reported in six thesis conducted by students at the Naval Postgraduate School [Refs: 1 through 6].

A. SCALING

The TJNAF FEL, which is capable of several hundred watts of continuous average power, was used to simulate the damage from a MW-class weapon by focusing the beam to a smaller spot size to increase intensity. The eventual goal is to develop scaling rules that will reliably predict the damage of a larger laser without having to bare the enormous cost of building the large laser first. The experimental data shows that the scaling concept with thermal diffusion calculations is promising. More detailed experiments varying wavelength, power, and spot size may be able to produce scaling laws, which would be invaluable for future weapons designers.

B. FEL PULSE FORMAT

The extremely short, sub-picosecond pulse length of the FEL beam is a result of the short electron bunches formed as they are accelerated in RF cavities. The TJNAF FEL has a unique pulse format with a rapid sequence of short, powerful pulses. The peak power in each pulse is about 100 MW lasting for only about one-half picosecond coming at a rate of 37 MHz. Other studies have shown that such ultra-short pulses may give as much as a factor of ten advantage in the reduced fluence required to produce damage [Ref. 25]. The experiments conducted for this report began to collect data intended to show whether this advantage exists. The results indicate that for a fixed average power level, a lower pulse repetition frequency with the corresponding higher power per pulse provides a faster burn through rate. This is probably because the lower PRF pulses contained enough fluence per pulse to immediately vaporize the material as well as raising it to the melting temperature.

The experiments also show that the requirement for the laser spot to be larger than the thermal diffusion length is a valid requirement, and that the burn through rate increases dramatically as the laser beam radius to thermal diffusion length ratio moves from marginal to large. If this requirement is not met the results of the experiment

might be far less than what would actually occur with a real weapon size laser.

C. FUTURE EXPERIMENTS

The TJNAF FEL is scheduled for an upgrade to 10 kW of power. This increase will allow more flexibility in scaling experiments and further tests of scaling itself. Additional experiments that include weighing of the samples before and after each run, new wavelengths, changing wavelengths during irradiation, new pulse formats, and other sample materials would be beneficial. As experimental procedures are refined and the amount of data increases, a more thorough analysis of the FEL damage results and comparison to other lasers will become possible.

When higher laser power is available in the future, the same irradiations should be conducted with bigger spot radii in order to compare the results and establish a scaling law. It is suggested that thicker samples should also be tested in order to determine if the penetration rate stays the same after the laser beam has penetrated the material a few mm. Samples should be machined to be no larger than the laser spot so that thermal diffusion cannot occur. Also, machining the samples to resemble the nosecone shape may be important.

Furthermore, a procedure for making the measurements of burn through times more accurate should be established, as they are very important in determining penetration depth rates. From the analysis of the results it appears that there is a strong relationship between the penetration depth rate and the laser intensity. When the intensity changed by a factor of 20 ($500\ W/cm^2 \rightarrow 10\ kW/cm^2$) the penetration depth rate also changed by almost the same factor in both samples.

VII. REFERENCES

1. Thomson, R.W., JR., "Experimental Damage Studies for a Free Electron Laser Weapon", Masters Thesis, Naval Postgraduate School, June 1999.

2. Short, L.R., "Damage Produced by the Free Electron Laser", Master's Thesis, June 1999.

3. Herbert, P. A. Herbert, "Anti-Ship Missile Defense and the Free Electron Laser", Master's Thesis, December 1998.

4. Dimitrios, D.L., Master's Thesis, December 2000.

5. Adamantios, C., Master's Thesis, December 2000.

6. McGinnis, R.D., "The Free Electron Laser for Directed Energy", Doctoral Dissertation, December 2000.

7. Kittel, C. "Introduction to Solid State Physics", 5th Edition, John Wiley and Sons, 1976.

8. Woehler, K.E., PH 4054 Course Notes, Naval Postgraduate School, 1998.

9. Schriempf, J. T., "Response of Materials to Laser Radiation: A Short Course", Naval Research Laboratory, Washington, D.C., July 1979.

10. Ang, L.K., et al., "Surface Instability of Multipulse Laser Ablation on a Metallic Target", Journal of Applied Physics, April 1998, Vol. 83, No. 8.

11. Stuart, B.C., et al., "Nanosecond to Femtosecond Laser Induced Breakdown in Dielectrics", Physical Review Letters, Vol., 53, No. 4., January 1996.

12. Anisimov, S.I., et al., "Electron emission from metal surfaces exposed to ultrashort laser pulses", Sov. Phys. JETP, August 1974, Vol. 39, No.2.

13. Allen, P.B., "Theory of Thermal Relaxation of Electrons in Metals", Physical Review Letters, September 1987, Vol. 59, No.13.

14. Corkum, P.B., et al., "Thermal Response of Metals to Ultrashort-Pulse Laser Excitation", Physical Review Letters, December 1988, Vol. 61, No. 25.

15. Sparks, M. Journal of Applied Physics, 1976, Vol. 47, p. 837.

16. Figueira, J.F., and Thomas, S.J., IEEE Journal of Quantum Electronics, 1982, Vol. 18, p. 1381.

17. Du, D., et al., "Laser-induced breakdown by impact ionization in SiO_2 with pulse widths from 7 ns to 150 fs", Applied Physics Letters, March 1987, Vol. 74, No. 12.

18. Shinn, M.D., Private Communication, (Letter dated 13 May 1999.

19. Small, D.W., "Interaction of Laser Beams with Relativistic Electrons," Doctoral Dissertation, Naval Postgraduate School, March 1997.

20. Powell, J.B., CAPT, USN, Private Communication, 18 October, 2000.

21. Wenzel,D. Naval Research Laboratory, Electronic Mail, 16 March 1999.

22. Shinn, M.D., Private Communication, (Letter dated 4 March 1999).

23. Shinn, M.D., Private Communication, (Letter dated 3 November 1999).

24. Shinn, M.D., Private Communication, (Letter dated 7 May 2000).

25. Stuart, B.C., et al, "Optical Ablation by High Power Short Pulse Lasers", Journal of the Optical Society of America., 1996.

VIII. INITIAL DISTRIBUTION

1.	Defense Technical Information Center 8725 John J. Kingman Rd., STE 0944 Ft. Belvoir, VA 22060-6218	2
2.	Dudley Knox Library Naval Postgraduate School 441 Dyer Rd. Monterey, CA 93943-5101	2
3.	Research Office, Code 09 Naval Postgraduate School Monterey, CA 93943	1
4.	Professor William B. Colson, Code PH/Cw Naval Postgraduate School Monterey, CA 93943-5117	2
5.	Commander Roger D. McGinnis 10 Mervine Street Monterey, CA 93940	1
6.	Lieutenant Commander Robert W. Thomson Jr. 11132 Swanson Ct. San Diego, CA 92131	1
7.	Lieutenant Lee R. Short 707 Seneca Street A-5 Ventura, CA 93001	1
8.	Lieutenant Commander Paul A. Herbert 474-A Ehako Place Honolulu, Hawaii 96817	1
9.	A. Christodoulou 12 Valtetsiou St Kaminia Piraeus 18540 Greece	1
10	Dimitrios Lampiris LOC Ikarias Rd. Mortero-Nea Erythrea Athens - 14671 Greece	1

10. Michelle Shinn 1
TJNAF
1200 Jefferson Ave.
Newport News, VA 23606

11. Steve Benson 1
TJNAF
1200 Jefferson Ave.
Newport News, VA 23606

12. George Neil 1
TJNAF
1200 Jefferson Ave.
Newport News, VA 23606

13. Dick Wenzel 1
Naval Research Laboratory
4555 Overlook Drive., SE
Washington, DC 20375-5000